



**HAL**  
open science

## Paleosecular Variation and the Time-Averaged Geomagnetic Field Since 10 Ma

Wellington Oliveira, Gelvam Hartmann, Filipe Terra-Nova, Daniele Brandt,  
Andrew Biggin, Yael Engbers, Richard Bono, Jairo Savian, Daniel Franco,  
Ricardo Trindade, et al.

► **To cite this version:**

Wellington Oliveira, Gelvam Hartmann, Filipe Terra-Nova, Daniele Brandt, Andrew Biggin, et al..  
Paleosecular Variation and the Time-Averaged Geomagnetic Field Since 10 Ma. *Geochemistry, Geo-  
physics, Geosystems*, 2021, 22 (10), 10.1029/2021GC010063 . hal-04054393

**HAL Id: hal-04054393**

**<https://hal.science/hal-04054393>**

Submitted on 1 Apr 2023

**HAL** is a multi-disciplinary open access archive for the deposit and dissemination of scientific research documents, whether they are published or not. The documents may come from teaching and research institutions in France or abroad, or from public or private research centers.

L'archive ouverte pluridisciplinaire **HAL**, est destinée au dépôt et à la diffusion de documents scientifiques de niveau recherche, publiés ou non, émanant des établissements d'enseignement et de recherche français ou étrangers, des laboratoires publics ou privés.



Distributed under a Creative Commons Attribution 4.0 International License



## RESEARCH ARTICLE

10.1029/2021GC010063

# Paleosecular Variation and the Time-Averaged Geomagnetic Field Since 10 Ma

### Key Points:

- An updated 0–10 Ma database provides improvements in the geographic and temporal distributions of high-quality data
- We propose a zonal time-averaged field model for the past 10 Myr
- Quantitative analyses suggest equatorial asymmetry of Brunhes chron paleosecular variation

Wellington P. de Oliveira<sup>1</sup> , Gelvam A. Hartmann<sup>1</sup> , Filipe Terra-Nova<sup>2</sup> ,  
Daniele Brandt<sup>2</sup> , Andrew J. Biggin<sup>3</sup> , Yael A. Engbers<sup>3</sup> , Richard K. Bono<sup>3</sup> ,  
Jairo F. Savian<sup>4</sup> , Daniel R. Franco<sup>5</sup> , Ricardo I. F. Trindade<sup>2</sup> , and  
Thiago R. Moncinhatto<sup>2</sup> 

<sup>1</sup>Instituto de Geociências, Universidade Estadual de Campinas, Campinas, Brazil, <sup>2</sup>Departamento de Geofísica, Instituto de Astronomia, Geofísica e Ciências Atmosféricas, Universidade de São Paulo, São Paulo, Brazil, <sup>3</sup>Department of Earth, Ocean and Ecological Science, University of Liverpool, Liverpool, UK, <sup>4</sup>Instituto de Geociências, Universidade Federal do Rio Grande do Sul, Porto Alegre, Brazil, <sup>5</sup>Coordenação de Geofísica, Observatório Nacional, Rio de Janeiro, Brazil

### Supporting Information:

Supporting Information may be found in the online version of this article.

### Correspondence to:

W. P. de Oliveira,  
[weloliveira@ige.unicamp.br](mailto:weloliveira@ige.unicamp.br)

### Citation:

de Oliveira, W. P., Hartmann, G. A., Terra-Nova, F., Brandt, D., Biggin, A. J., Engbers, Y. A., et al. (2021). Paleosecular variation and the time-averaged geomagnetic field since 10 Ma. *Geochemistry, Geophysics, Geosystems*, 22, e2021GC010063. <https://doi.org/10.1029/2021GC010063>

Received 26 JUL 2021

Accepted 16 SEP 2021

**Abstract** Investigations into long-term geomagnetic variations provide useful information regarding paleomagnetic field behavior. In this study, we assess the latitudinal structure of paleosecular variation (PSV) and the time-averaged field (TAF) for the Brunhes normal and Matuyama reverse chrons, and for the 0–10 Ma period, from an updated and reviewed paleodirectional database spanning the past 10 Myr. The new database comprises 2,543 paleomagnetic sites from igneous rocks, providing improvements in the geographic and temporal distributions of high-quality data relative to previous compilations. In addition, the new data collection differs considerably in application of strict selection criteria. Statistical analysis of the virtual geomagnetic pole (VGP) dispersion curve of Model G reveals a low latitudinal dependence of PSV for the last 10 Myr. For this period, we present a zonal TAF model based on the latitudinal distribution of inclination anomaly data. The best estimates found for axial quadrupole and octupole components were about 3% and 1% relative to axial dipole component, respectively. The new statistical models for the Brunhes and Matuyama chrons have different patterns in both PSV and TAF, in compliance with earlier studies. Our quantitative assessments indicate an apparent hemispheric PSV asymmetry, particularly in the Brunhes chron, with a stronger latitudinal signature in the southern hemisphere compared to the north. These findings suggest that equatorial PSV asymmetry, that has previously been found in modern, historical and millennial scale geomagnetic models, has persisted over the past 0.78 Ma.

## 1. Introduction

Spatial and temporal geomagnetic field variations have been observed over different geological timescales. Ancient field measurements, mainly obtained from geological materials (sedimentary and igneous rocks), allow investigations of directional and intensity variability of the paleomagnetic field that result from processes operating in Earth's fluid core (see, e.g., Hulot et al., 2010). Particularly, information about paleosecular variation (PSV), long-term variations of the order of  $10^5$ – $10^6$  years (e.g., Johnson & McFadden, 2015), is essential to better understand temporal geomagnetic field evolution and to constrain numerical geodynamo models (Biggin et al., 2020; Coe & Glatzmaier, 2006; Davies et al., 2008; Meduri et al., 2021; Sprain et al., 2019). On these long timescales, a basic assumption of paleomagnetism concerns the time-averaged field (TAF) structure, which can be described approximately by a geocentric axial dipole (GAD) where the dipole aligns with Earth's spin axis (Merrill & McFadden, 2003).

PSV and TAF studies have focused on the 0–5 Ma interval because of the large availability of paleodirectional data relative to earlier epochs, and due to the reduced effects of plate tectonic motion. Various global paleomagnetic databases for lava flows and thin dykes data (e.g., Johnson et al., 2008; Lee, 1983; McElhinny & McFadden, 1997; McElhinny & Merrill, 1975) have been developed to construct PSV and TAF models. The main differences among 0–5 Ma databases relate to the selection criteria adopted (see Johnson and McFadden [2015] for a detailed review). Additionally, data collections are affected by poor spatial and temporal coverage and low-quality data. As addressed by some authors (e.g., Johnson et al., 2008; McElhinny & McFadden, 1997), these factors can influence PSV and TAF modeling, and make it difficult to

© 2021. The Authors.

This is an open access article under the terms of the [Creative Commons Attribution License](https://creativecommons.org/licenses/by/4.0/), which permits use, distribution and reproduction in any medium, provided the original work is properly cited.

understand paleofield behavior. Over the past two decades, significant progress has been achieved in obtaining high-quality data for the last 10 Myr (Cromwell et al., 2018; Johnson et al., 2008; Opdyke et al., 2015). These studies imposed rigorous selection criteria for obtaining acceptable data, requiring improved statistical parameters and determined from modern laboratory methods. In essence, these high-quality data compilations provide support for statistical investigations of non-GAD field contributions, detection of distinctions between normal and reverse polarity fields, and evaluation of possible hemispheric asymmetries in PSV and TAF estimates.

PSV is usually assessed by the angular dispersion of virtual geomagnetic poles (VGPs) assuming a GAD field (Merrill & McFadden, 2003). The latitudinal variation in VGP dispersion has been described by two main types of statistical PSV models: Model G (McFadden et al., 1988) and Giant Gaussian Process (GGP) models (Constable & Parker, 1988). These models were designed based on observable modern geomagnetic field properties, but use different statistical approaches. Both models consider the surface magnetic field in spherical harmonic form, where Gauss coefficients  $g_l^m$  and  $h_l^m$  ( $l$  is the degree and  $m$  is the order) define the field geometry. In the phenomenological Model G of McFadden et al. (1988), the overall VGP angular dispersion ( $S$ ) is composed of two independent dynamo families, known as primary (or antisymmetric) and secondary (or symmetric) families, expressed by:

$$S(\lambda) = \sqrt{S_s^2 + S_p^2}. \quad (1)$$

The contribution relative to the primary family ( $S_p$ ) comprises spherical harmonic terms with odd-numbered  $l - m$  (i.e., equatorially antisymmetric terms), which was assumed to vary linearly with latitude ( $\lambda$ ). The secondary family ( $S_s$ ) that contributes to the VGP dispersion is given by the equatorially symmetric terms for which  $l - m$  is even and is assumed to be approximately constant for all latitudes. In this respect, Model G can be described by a latitudinal variation curve fitted to the dispersion data, considering two shape parameters  $a$  ( $= S_s$ ) and  $b$  ( $= S_p/\lambda$ ), respectively, which are related to the secondary and primary families (McElhinny & McFadden, 2000).

GGP-type models offer a different statistical perspective capable of predicting the distribution of geomagnetic field vectors in any geographical location, by describing the variances of Gauss coefficients. Initially defined by Constable and Parker (1988) who considered each Gauss coefficient as a normally distributed random variable, and the prescribed variances that reproduce the spatial power spectrum (Lowe, 1974) of the modern field. All non-dipole spherical harmonic terms have zero mean except for the axial quadrupole component. Prior to 2020, four GGP models: CP88 (Constable & Parker, 1988), QC96 (Quidelleur & Courtillot, 1996), CJ98 (Constable & Johnson, 1999), and TK03 (Tauxe & Kent, 2004) were presented, and are differentiated by the analytical methods and paleomagnetic 0–5 Ma database used (see Johnson & McFadden, 2015). Recently, the GGP models of BCE19 (Brandt et al., 2020), BB18 and BB18.Z3 (Bono et al., 2020) have been used to evaluate the latitudinal behavior of PSV spanning the last 10 Myr using the 0–10 Ma database (hereafter PSV10) of Cromwell et al. (2018). The BCE19 model was constructed from analysis of paleodirectional data, taking into account the shape and dispersion of directional distributions at any latitude. It assumes that only the axial dipole term  $\bar{g}_1^0$  has a non-null mean value, and the variances ( $\sigma_l^{m^2}$ ) of any Gaussian coefficients depend on the degree  $l$  and  $m$ , and the parameters  $\alpha$  and  $\beta$ , respectively, which are associated with the secondary and primary family coefficients (following the formulation of the TK03 model). The BB18-family models introduce a covariance between the Gauss coefficients for a specific set of terms with degrees  $l \leq 4$  deduced from numerical geodynamo simulations. The BB18 model considers only a mean  $\bar{g}_1^0$  term, while the BB18.Z3 model includes the axial quadrupolar  $\bar{g}_2^0$  and octupolar  $\bar{g}_3^0$  terms. In addition, BB18 models improve the fit to the latitudinal dependence of VGP dispersion estimates and the paleointensity records for the last 10 Myr.

Regarding the TAF geometry, the presence of non-GAD components over the past few million years has been debated (Aubert et al., 2010). Through analyses of the latitudinal distribution of inclination anomaly ( $\Delta I$ ) data, zonal TAF models for the 0–5 Ma period (McElhinny et al., 1996; Merrill & McElhinny, 1977; Merrill et al., 1990) indicate that the prominent component is the axial quadrupole term ( $g_2^0 \sim 4\%$  of  $g_1^0$ ), with a small octupole contribution ( $g_3^0 \sim 1\%$  of  $g_1^0$ ). In addition, higher PSV estimates and larger non-dipole

contributions were reported for reverse polarity periods compared to normal polarity periods (Johnson et al., 2008; McElhinny & McFadden, 1997).

A further debate concerns potential hemispheric paleomagnetic field asymmetries (Cromwell et al., 2013; Engbers et al., 2020). In particular, the latitudinal PSV structure for the past few million years suggests higher southern hemisphere VGP dispersion than northern hemisphere (Cromwell et al., 2013, 2018; Lawrence et al., 2009). Predictions from numerical geodynamo simulations indicate that lateral thermal variations at the core-mantle boundary (CMB) could influence geomagnetic field morphology and promote asymmetries (Aubert et al., 2013; Davies et al., 2008; Terra-Nova et al., 2019). However, our knowledge of long-lived PSV and TAF asymmetries is limited by the uneven temporal and geographic sampling of paleomagnetic records. In this context, improvements and expansion to the current 0–10 Ma database are important to better assess the TAF structure, and to constrain Earth-like geodynamo models.

Here we review and update the paleodirectional database derived from igneous rocks for the past 10 Myr using stringent selection criteria compared to the previous compilations. We then evaluate the latitudinal PSV and TAF structure for three age intervals corresponding to the Brunhes and Matuyama chrons, and the 0–10 Ma period. VGP dispersion estimates from Model G are compared with recent PSV studies and with the BCE19 and BB18 model family. We also quantitatively assess VGP dispersion patterns for the northern and southern hemispheres and extend investigations for the historical period from the COV-OBS geomagnetic field model (Gillet et al., 2015). We present new zonal TAF models for each age interval based on robust inclination anomaly estimates, and discuss the presence of non-dipole components relative to the GAD term.

## 2. Paleomagnetic Database

In order to investigate PSV behavior and TAF structure in the 0–10 Ma interval, we compiled an updated database of high-quality paleodirections from published studies. They include: the Magnetics Information Consortium (MagIC) database (<https://www2.earthref.org/MagIC>; Tauxe et al., 2016), academic search engines (e.g., *Scopus* at <https://www.scopus.com/home.uri>), and the PSV10 compilation (Cromwell et al., 2018). Only paleomagnetic data derived from volcanic rocks and thin dykes were accepted because these are considered most suitable for PSV and TAF analysis, and they provide instantaneous paleomagnetic field records in contrast to smoothed sedimentary records (Johnson & McFadden, 2015). We further employ the following selection criteria.

1. All paleomagnetic data must be within the age interval 0–10 Ma.
2. The characteristic remanent magnetization (ChRM) directions must have been acquired using modern demagnetization procedures and processing techniques. Additionally, site-level data must have an associated *demagnetization code* (the number of demagnetization site used for ChRM determination) equal to four or five ( $DC \geq 4$ , McElhinny & McFadden, 2000).
3. Studies that did not provide site-mean directions and site coordinates were rejected.
4. Studies where the sampling region has been subjected to significant post-emplacement tectonism (e.g., tilting) were not included, based on information provided in the original publications.
5. All studies must comprise paleodirectional data from at least 10 sites (i.e.,  $N \geq 10$ ) related to independent geomagnetic field records, for a given study location.
6. We require a minimum of five samples per site ( $n \geq 5$ ), with an estimated Fisher precision parameter (Fisher, 1953) of  $k \geq 50$  for each site-mean direction.

Detailed discussion of these six selection criteria can be found in Text S1 in Supporting Information S1.

The paleomagnetic database contains 2,543 directional sites from 80 paleomagnetic studies published between 1989 and 2020 that meet our selection criteria. Selected data sets associated with their respective geographic locations, average ages, DC values, and references are listed in Table S1. Moreover, our compilation supplies additional information for all site-level data (summarized in Table S2), including site coordinates, paleolocations (computed using the NNR-MORVEL 56 model (Argus et al., 2011) for plate motion corrections), Fisher site-mean directions, paleomagnetic statistical parameters, ages, and VGP coordinates. We

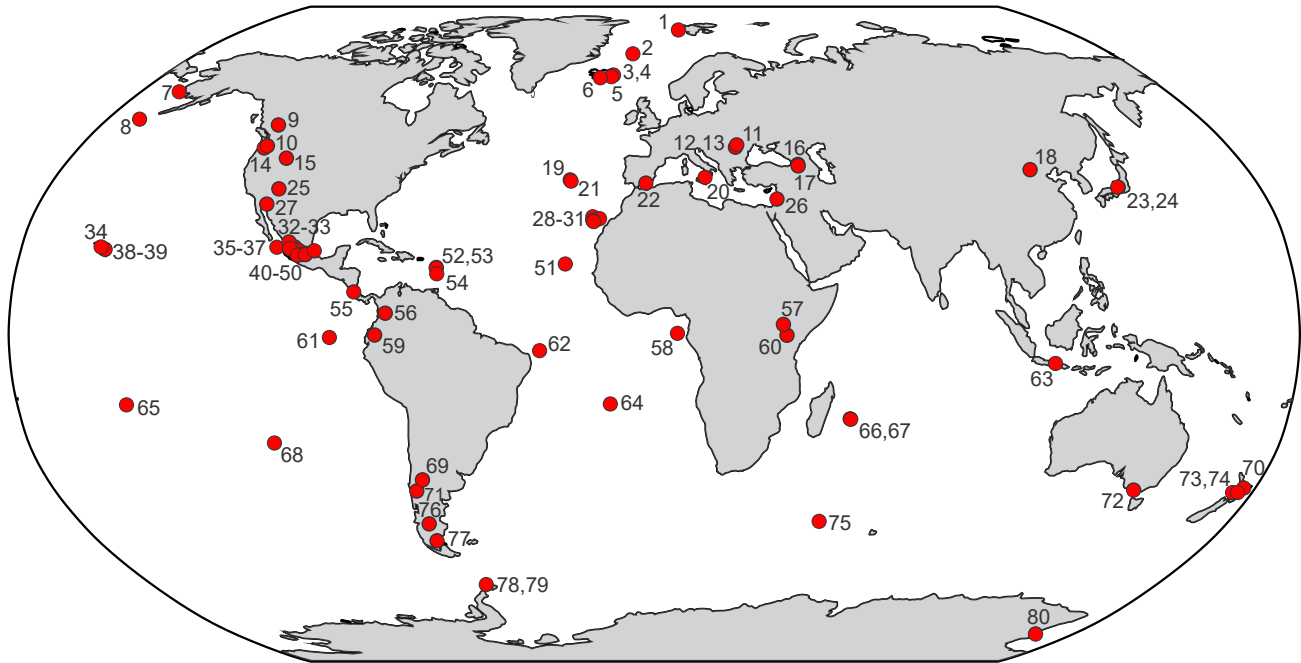


**Figure 1.** Global distribution of selected paleodirectional data over the past 10 Myr. Numbers represent identification numbers reported in Table S1.

consider here site locations corrected for plate tectonic motions in the PSV and TAF statistical analyses (as adopted by Cromwell et al. [2018]), as discussed below.

Regarding the number of paleomagnetic sites and quality criteria, the new database supersedes the PSV10 data set (as discussed in Section 5.1), and offers a latitudinal coverage from 78°S to 78°N (Figure 1). There is an uneven spatial distribution of paleodirectional data between the northern and southern hemispheres; the latter consists of 23 data sets which corresponds to 29% of the collection.

Most of paleodirectional data are associated with high-level demagnetization procedures ( $DC = 5$ ; 72% of the paleomagnetic sites; Table S2, Figure S1). The number of samples per site are mainly within the 5–10 range (~89% of sites), whereas the Fisher precision parameter,  $k$  is concentrated between 50 and 200. Only 844 paleodirectional sites (~33%) are associated with radiometric dating based on information from the original references. For other sites, average ages were inferred from stratigraphic and historic records discussed in selected studies. Paleomagnetic sites for last 10 Myr are mainly from the Brunhes (39%) and Matuyama (29%) chrons.

### 3. Methods

We examined the statistical behavior of the paleofield during three time periods similar to Johnson et al. (2008, hereafter J08): (a) the entire 0–10 Ma data sets, (b) Matuyama (0.78–2.58 Ma) reverse polarity data, and (c) Brunhes (0–0.78 Ma) normal polarity data. We aim to ascertain whether there are differences between normal and reverse polarity intervals. Data sets assigned to the Gauss and Gilbert chrons were not assessed due to insufficient data to perform a separate analysis for these time intervals.

#### 3.1. Estimate of Paleosecular Variation

To assess PSV behavior, the between-site dispersion ( $S_B$ ) for each data set was calculated according to (McElhinny & McFadden, 1997):

$$S_B = \sqrt{S^2 - \frac{S_w^2}{\bar{n}}}, \quad (2)$$

First, it is necessary to calculate the total angular VGP dispersion ( $S$ ) given by (Cox, 1970):

$$S = \sqrt{\frac{1}{N-1} \sum_{i=1}^N \Delta_i^2}, \quad (3)$$

where  $N$  is the number of sites and  $\Delta_i$  corresponds to the angular deviation between the  $i$ th VGP and the mean VGP. All VGP data associated with reverse polarity directions were converted to normal poles before calculating  $S$  values.

In Equation 2, the correction factor ( $S_w^2/\bar{n}$ ) is used to remove random errors associated with the within-site dispersion, which is expressed by:

$$\frac{S_w^2}{\bar{n}} = 0.335 \bar{\alpha}_{95}^2 \frac{2(1 + 3 \sin^2 \lambda)^2}{(5 + 3 \sin^2 \lambda)}, \quad (4)$$

where  $\bar{n}$  is the average number of samples at each site;  $\bar{\alpha}_{95}$  represents the average 95% confidence cone about the site-mean direction for a specific data set, and  $\lambda$  is the site mean latitude.

To investigate the latitudinal variation of  $S_B$  data, we used Model G (McFadden et al., 1988), which describes the latitudinal dependence of VGP dispersion curves by:

$$S_B(\lambda) = \sqrt{a^2 + (b\lambda)^2}, \quad (5)$$

where  $a$  and  $b$  are empirical constants related to the symmetric ( $S_s = a$ ) and antisymmetric ( $S_p = b\lambda$ ) geodynamo families, respectively. Shape parameters  $a$  and  $b$  values were estimated by fitting to  $S_B$  data using a Python-based algorithm (defined with the *scipy.optimize.leastsq* package) that employs the Levenberg-Marquardt method, which is suitable for solving nonlinear least squares regressions (Aster et al., 2012), and has been used in two recent PSV studies (de Oliveira et al., 2018; Franco et al., 2019).

### 3.2. Estimate of the Time-Averaged Paleomagnetic Field

For analysis of the latitudinal structure of the 0–10 Ma TAF, we calculate the inclination anomaly ( $\Delta I$ ) that is the difference between observed inclination ( $I_{\text{OBS}}$ ) and the inclination expected for a GAD field, following Cox (1975):

$$\Delta I = I_{\text{OBS}} - I_{\text{GAD}}. \quad (6)$$

Before calculating  $\Delta I$ , reverse polarity site-mean directions were converted to antipodal directions. Thus,  $\Delta I$  values for each data set were estimated by the difference between the mean inclination (Fisher, 1953) and the GAD inclination ( $I_{\text{GAD}}$ ), calculated from the site mean latitude  $\lambda$ :

$$I_{\text{GAD}} = \tan^{-1}(2 \tan \lambda). \quad (7)$$

The distribution of  $\Delta I$  anomalies allows estimation of the zonal quadrupole ( $g_2^0$ ) and octupole ( $g_3^0$ ) contributions relative to the axial dipole term ( $g_1^0$ ) from the predicted field model for observed inclination ( $I_{\text{obs}}^*$ ) as a function of colatitude  $\theta$  ( $90^\circ - \text{latitude}$ ) given by (McElhinny et al., 1996):

$$\tan(I_{\text{obs}}^*) = \frac{2 \cos \theta + G2 \left( \frac{9}{2} \cos^2 \theta - \frac{3}{2} \right) + G3 (10 \cos^3 \theta - 6 \cos \theta)}{\sin \theta + G2 (3 \cos \theta \sin \theta) + G3 \left( \frac{15}{2} \cos^2 \theta \sin \theta - \frac{3}{2} \sin \theta \right)}. \quad (8)$$

We determined the zonal quadrupole ( $G2 = g_2^0/g_1^0$ ) and octupole terms ( $G3 = g_3^0/g_1^0$ ) by weighted least squares fittings between the observed  $\Delta I$  anomalies and the predicted inclination anomaly (from Equations 6–8), where the weighting factors correspond to 95% uncertainties in the observed  $\Delta I$  data. The best-fit TAF model was obtained based on the Levenberg–Marquardt method (see Section 3.1).

### 3.3. Transitional VGPs

Anomalous VGP data (characterized by large deviations from the mean pole) are generally excluded in PSV and TAF studies to ensure that data reflect stable field regimes. These anomalous VGPs (also referred to as outliers; Biggin et al., 2008) can be associated with geomagnetic excursions, polarity transitions, or spurious data caused by experimental measurement errors or secondary magnetizations (Johnson & McFadden, 2015). To evaluate the effects of transitional data on PSV and TAF estimates, we calculate the dispersion  $S_B$  and  $\Delta I$  after applying three approaches for each time period. The first applied no VGP cutoff and considered all directional data. The second used a fixed  $45^\circ$  cutoff angle, removing paleodirectional sites with VGPs that deviate  $>45^\circ$  from the mean paleomagnetic pole. The third used the criterion of Vandamme (1994), where the cutoff angle ( $A$ ) relative to mean pole is calculated as a function of dispersion  $S$ , by:

$$A = 1.8 S + 5^\circ. \quad (9)$$

An iterative method is employed according to the  $A$  value for a given data set; if VGP data are larger than the  $A$  estimate, they are excluded,  $S$  is recalculated, and the procedure is repeated until there are no larger deviations than the value determined from Equation 9.

Approximately 3% of paleodirectional sites from the entire 0–10 Ma data set are regarded as anomalous or transitional after applying a fixed  $45^\circ$  cutoff; this increased to 5% for the Vandamme (1994) criterion. The statistical distribution of paleomagnetic sites retained after applying a VGP cutoff for the three time periods is shown in Figure S2.

## 4. Results

### 4.1. Analysis of Latitudinal Variation of VGP Dispersion

$S_B$  estimates for three temporal subsets: 0–10 Ma, Matuyama, and Brunhes age intervals are presented in Tables S3–S5, respectively. Tables S3–S5 also include, for each age group,  $S_B$  results with lower and upper 95% confidence limits determined by the bootstrap method (Efron & Tibshirani, 1993), alongside values of average site latitude and longitude, mean direction, corresponding paleomagnetic pole, and paleomagnetic statistical parameters. Some data sets have substantially higher or lower  $S_B$  estimates, so we apply an additional criterion proposed by Deenen et al. (2011) to assess whether the data adequately sample PSV, which is defined by an envelope  $A_{95}$  limited by a range of values between  $A_{95\min}$  and  $A_{95\max}$  (see Text S2 in Supporting Information S1). This criterion was used to identify data with extremely different behaviors from that generally observed in paleomagnetic studies; these data were not considered in our PSV and TAF analyses. Furthermore, this criterion was used here because it was designed for datasets and models from targets with ages of a few million years and with thermoremanence acquisition similar to those found here, that is, data derived from rapidly cooling igneous rocks. In the 0–10 Ma period, we identify a maximum of 11 data sets that do not meet the criterion of Deenen et al. (2011; see Table S3). These possible PSV estimate biases may be related to transitional data that are over-represented in some data sets, especially when no VGP cutoff or a variable cutoff is employed (data sets # 5, 12, 22, 31, 76, and 80). In addition, data that are serially correlated or that are temporally underrepresented may contribute to anomalously low  $S_B$  values in three paleomagnetic studies (data sets # 32, 39, and 48). Another relevant factor might be undetected regional tectonic effects that can enhance  $S_B$  estimates.

For analysis of latitudinal variation of VGP dispersion, following the assumption of Model G that PSV is hemispherically symmetric,  $S_B$  values for northern and southern hemispheres (represented by closed and open symbols, respectively, in Figures 2b–2d to 4b–4d) are plotted on the same axis as a function of absolute latitude value. Curves for Model G are first presented for the 0–10 Ma data (Figure 2), and then for the Matuyama and Brunhes subsets separately (Figures 3 and 4, respectively). Shape parameters  $a$  and  $b$  estimates and their 95% confidence limits for the three time periods are summarized in Table 1. Furthermore, the  $S_B$  data distribution is compared with three recent GGP models: BCE19, BB18, and BB18.Z3. The method employed for predicted dispersions is described in Text S3 in Supporting Information S1.

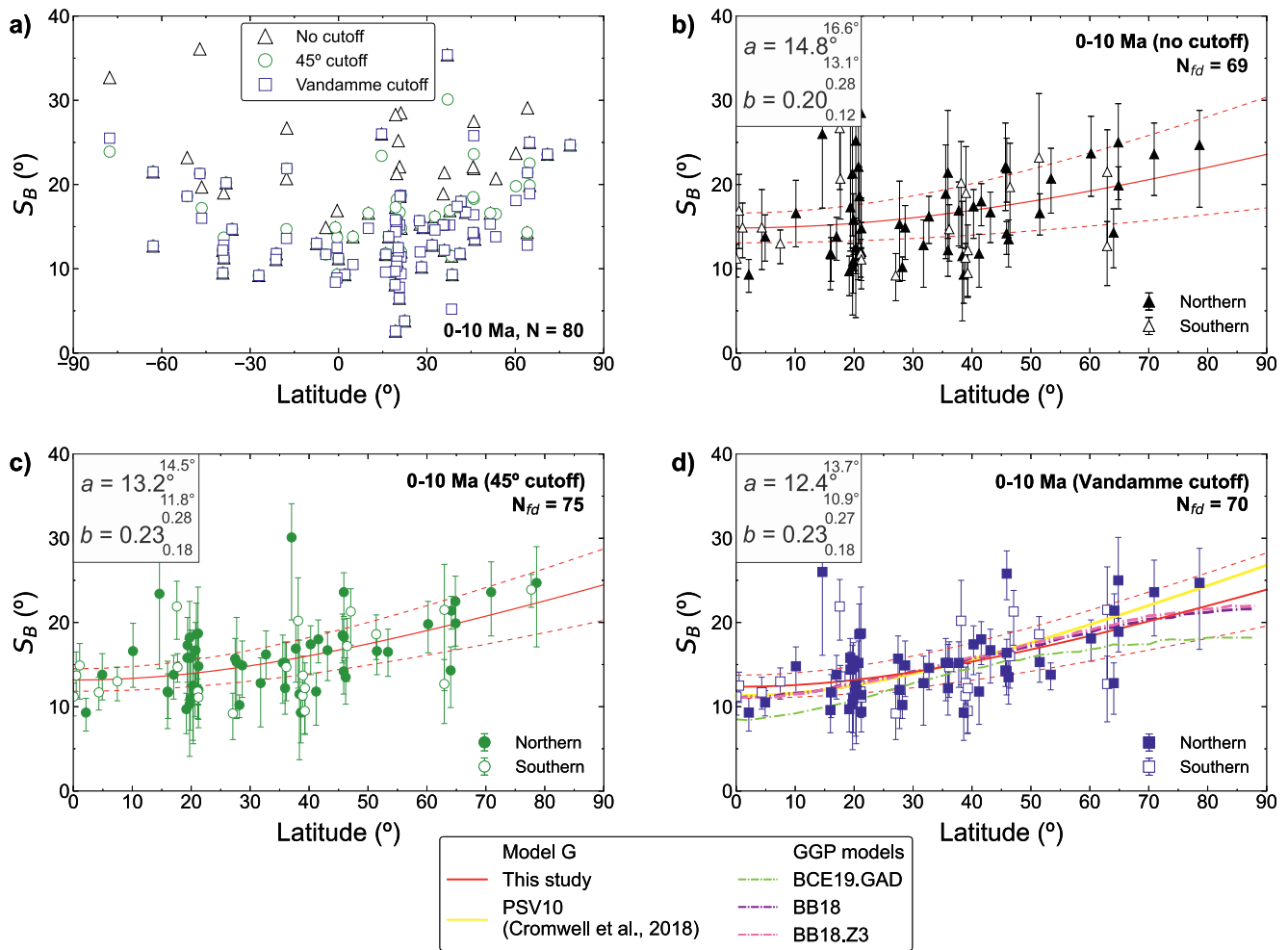


**Figure 2.** Virtual geomagnetic pole (VGP) dispersion ( $S_B$ ) as a function of latitude for (a) 0–10 Ma  $S_B$  results with interhemispheric coverage defined using three VGP cutoff approaches. (b–d)  $S_B$  estimates with 95% bootstrap confidence limits projected onto a single hemisphere. Closed (open) symbols correspond to data from the northern (southern) hemisphere. The best-fit Model G curves (McFadden et al., 1988) to  $S_B$  data are represented by red lines, associated with 95% confidence intervals (red dashed lines). (b) No cutoff applied, (c) 45° cutoff, and (d) Vandamme (1994) cutoff. In (d), the yellow line denotes the Model G curve fitted to the PSV10 data compilation (Cromwell et al., 2018). Also shown are VGP dispersions predicted for three GGP models: BCE19.GAD model of Brandt et al. (2020); light green dash-dot line; BB18 and BB18.Z3 models (Bono et al., 2020) purple and pink lines, respectively.

$S_B$  estimates for the 0–10 Ma interval (80 data sets, Table S3), defined using three VGP cutoff approaches, are displayed in an interhemispheric representation in Figure 2a. Overall, an increasing dispersion  $S_B$  trend can be observed as a function of latitude for both hemispheres. Differences in PSV estimates are identified when the fixed (45°) cutoff and Vandamme (1994) criterion exclude transitional data. Model G fits most  $S_B$  data reasonably well, regardless of the VGP cutoff employed (Figures 2b–2d).  $S_B$  data with no VGP cutoff (69 data sets, Figure 2b) produces a best-fit Model G curve with parameters  $a = 14.8^{16.6}_{13.1}$  and  $b = 0.20^{0.28}_{0.12}$ . Using the 45° cutoff angle (75 data sets, Figure 2c) yields a slight 1.6° decrease of parameter  $a = 13.2^{14.5}_{11.8}$ , while parameter  $b = 0.23^{0.28}_{0.18}$  is slightly higher than in Figure 2b. The Model G curve is also similar to the  $S_B$  data when subjected to the Vandamme (1994) cutoff (70 data sets, Figure 2d), and only differs in the value of  $a = 12.4^{13.7}_{10.9}$ , with  $b = 0.23^{0.27}_{0.18}$ . These two parameters are statistically compatible at the 95% confidence level in relation to the data filtered with a fixed 45° cutoff and with no cutoff. Dispersions predicted using the GGP models (Figure 2d) have low values compared to the Model G curve. The BB18 and BB18.Z3 models (purple and pink dash-dot lines, respectively) have lower dispersions at equatorial and high latitudes, while BCE19 (green dash-dot line) is lower at all latitudes. In addition, the BB18-family models better fit observed  $S_B$  data compared to the BCE19 model.

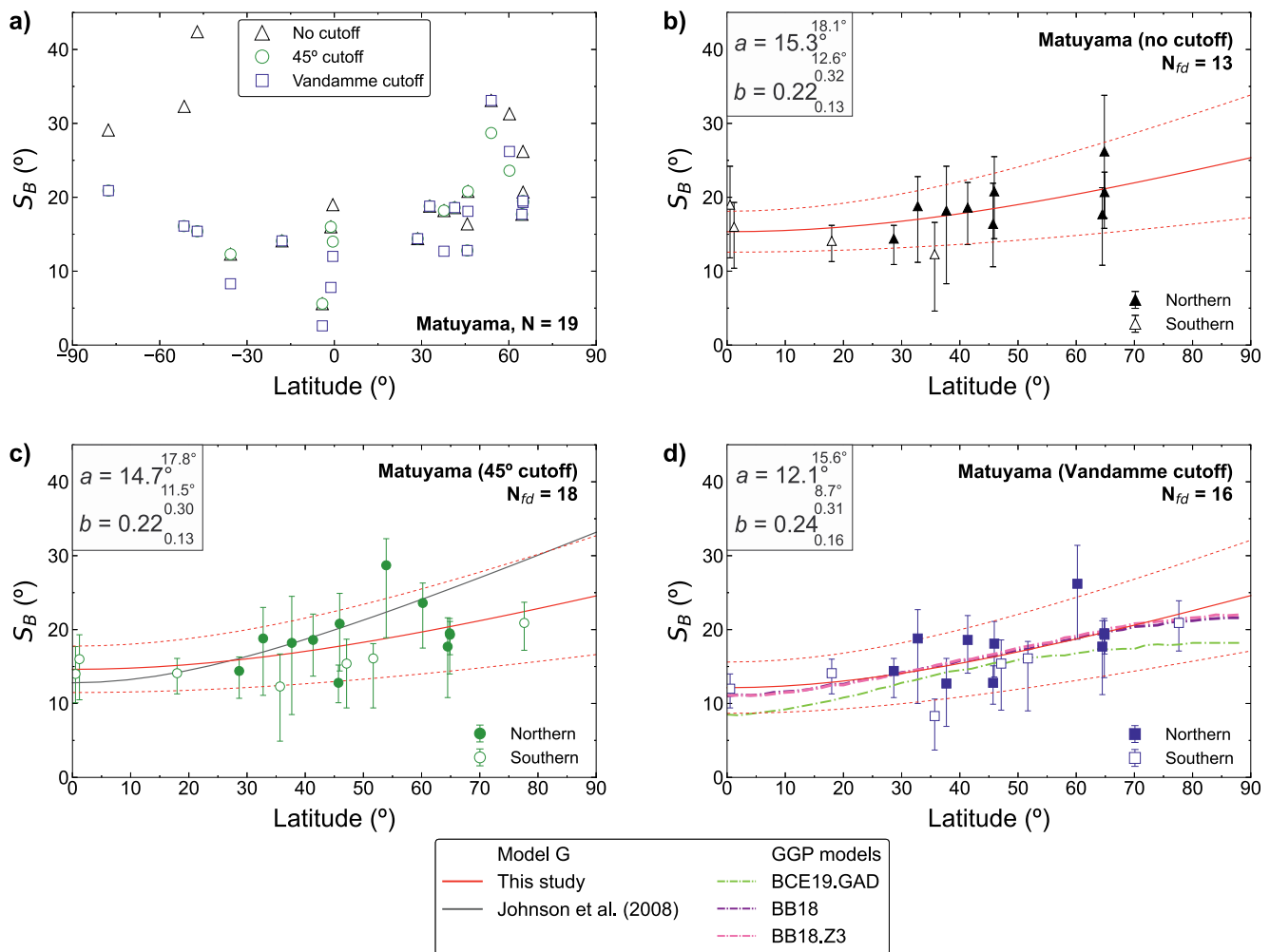


**Figure 3.** Virtual geomagnetic pole (VGP) dispersion ( $S_B$ ) as a function of latitude for the Matuyama reverse polarity chron. (a)  $S_B$  results with interhemispheric coverage defined using three VGP cutoff approaches. See Figure 2 caption for details. The gray line in (c) denotes the Model G curve fitted to the Matuyama data of Johnson et al. (2008).

For the Matuyama reversed polarity chron (19 data sets, Table S4), a pattern of increased  $S_B$  values is observed as a function of latitude for both hemispheres (Figure 3a). Nevertheless, there is a data gap at low (0–25°N) and high (>65°N) northern latitudes, and data coverage is even more restricted in the southern hemisphere. When a VGP cutoff (variable or fixed) is employed,  $S_B$  estimates are especially different for data sets from Antarctica at 78°S (Lawrence et al., 2009) and North America at latitudes 60°N (Coe et al., 2000), and 46°N (Lhuillier et al., 2017). Model G for data sets with no cutoff (13 data sets, Figure 3b) yields  $a = 15.3^{18.1^\circ}_{12.6^\circ}$  and  $b = 0.22^{0.32}_{0.13}$ . Applying the fixed 45° cutoff (18 data sets, Figure 3c) decreases  $a$  from 15.3° to  $14.7^{17.8^\circ}_{11.5^\circ}$  and  $b = 0.22^{0.30}_{0.13}$ , but these estimates are not statistically different considering the 95% confidence intervals. When the Vandamme (1994) criterion (16 data sets, Figure 3d) is used, Model G yields  $a = 12.1^{15.6^\circ}_{8.7^\circ}$  and  $b = 0.24^{0.31}_{0.16}$ , which are similar to those with no VGP cutoff. Considering the GGP models in Figure 3d, predicted VGP dispersion values for BB18-family models are lower at low and high latitudes compared to the Model G fit, whereas the BCE19 model has lower dispersion along the entire latitudinal range relative to the Model G. BB18 and BB18.Z3 models fit the  $S_B$  data better as a function of latitude compared to the BCE19 model.

The interhemispheric distribution of Brunhes normal polarity data (46 data sets, Table S5) is illustrated in Figure 4a. The northern hemisphere has good data coverage to 70°N, while the southern hemisphere presents a sparse data coverage, especially in mid- to high-latitudes (40°–60°S). Most studies have small differences in VGP dispersion when fixed or variable cutoffs are used. The best-fit curve for  $S_B$  estimates when no

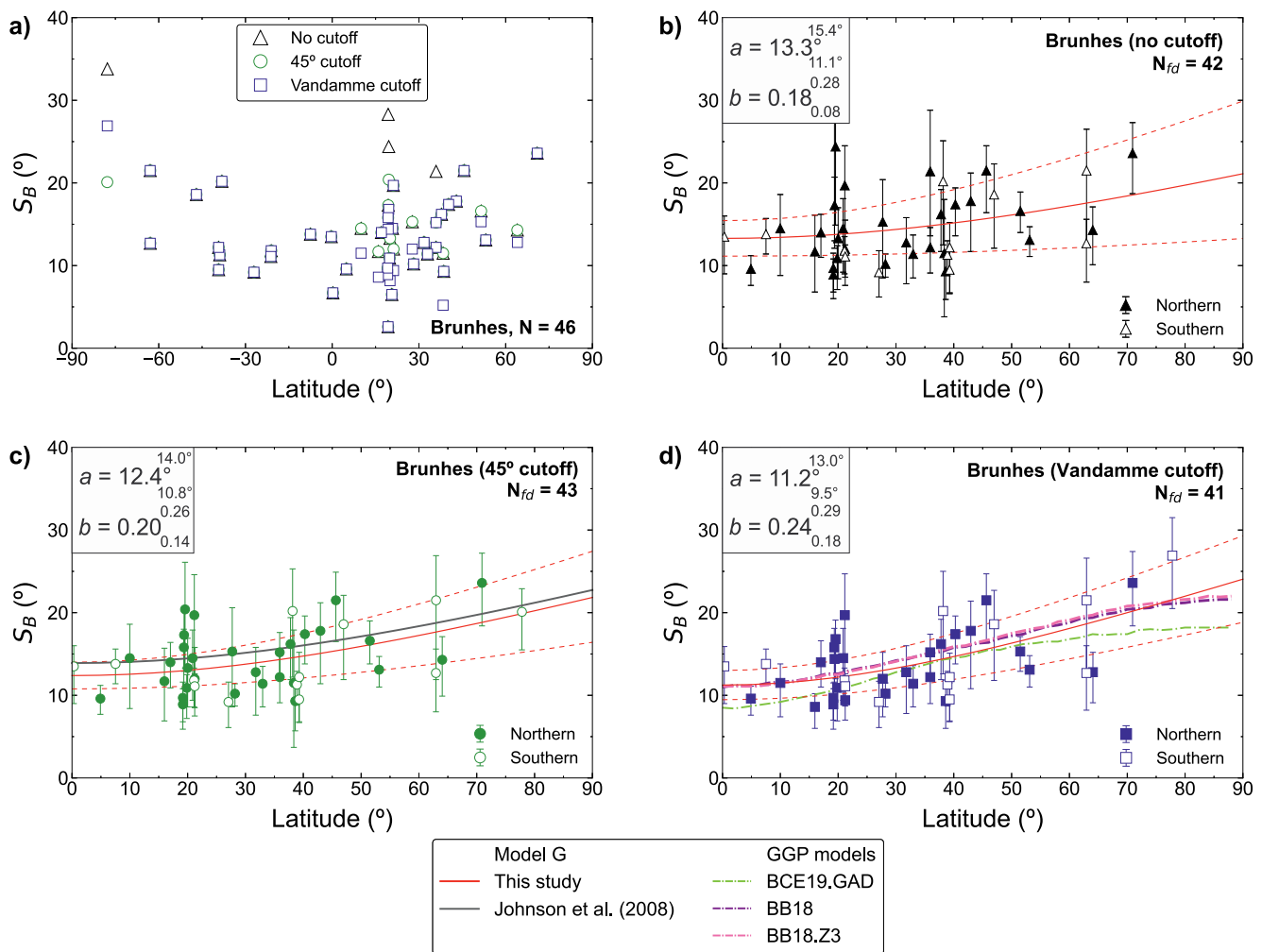


**Figure 4.** Virtual geomagnetic pole (VGP) dispersion ( $S_B$ ) as a function of latitude for the Brunhes normal polarity chron. (a)  $S_B$  results with interhemispheric coverage defined using three VGP cutoff approaches. See Figure 2 caption for details. The gray line in (c) denotes the Model G curve fitted to the Brunhes data of Johnson et al. (2008).

VGP cutoff is applied (42 data sets) for Model G yields  $a = 13.3^{15.4}_{11.1}^\circ$  and  $b = 0.18^{0.28}_{0.08}$  (Figure 4b). Applying a constant 45° cutoff (43 data sets, Figure 4c) and the Vandamme (1994) criterion (41 data sets, Figure 4d), estimated shape parameters are  $a = 12.4^{14.0}_{10.8}^\circ$ ,  $b = 0.20^{0.26}_{0.14}$  and  $a = 11.2^{13.0}_{9.5}^\circ$ ,  $b = 0.24^{0.29}_{0.18}$ , respectively. All Model G parameters are similar regardless of cutoff employed. Regarding the GGP models, predicted dispersions for BB18 and BB18.Z3 models are compatible with the observed  $S_B$  data in a broad range of latitudes, while the BCE19 model is compatible with some data at low to mid-latitudes. When GGP models are compared to the Model G curve, the expected dispersions for BB18-family models are slightly higher for latitudes from 20° to 70°, whereas the BCE19 Model provides lower dispersion estimates for all latitudes.

#### 4.2. Analysis of Latitudinal Structure of Inclination Anomaly

In general,  $\Delta I$  data for the 0–10 Ma interval (Table S3 and Figures 5a–5c) are not statistically distinguishable from the GAD field model (dashed line) at mid- to high-latitudes for both hemispheres, which contrasts with the large negative inclination anomalies at low latitudes (0–30°N and S). The best-fit field model for 0–10 Ma data without VGP cutoff (Figure 5a) yields estimates of  $G_2 = 0.037^{0.058}_{0.016}$  and  $G_3 = 0.015^{0.034}_{-0.005}$ . These values are statistically compatible with estimates  $G_2 = 0.035^{0.054}_{0.015}$  and  $G_3 = 0.018^{0.036}_{0.001}$  obtained with a fixed 45° cutoff (Figure 5b), and  $G_2 = 0.032^{0.050}_{0.014}$  and  $G_3 = 0.012^{0.028}_{-0.004}$  for subsets using the Vandamme (1994) cutoff (Figure 5c). Some data differ significantly from the predicted zonal field model within the 95%

**Table 1**  
Estimates of  $a$  and  $b$  Parameters for Model  $G$  and Estimates of the Zonal Quadrupole ( $G_2$ ) and Octupole ( $G_3$ ) Terms From This Study

PSV and TAF estimates	$N_{\text{fid}}$	$a_l^u$ ( $^\circ$ )	$b_l^u$	$G_2^u$	$G_3^u$
<b>0–10 Ma</b>					
$S_B$ and $\Delta I$ , no cutoff	69	14.8 <sup>16.6</sup> <sub>13.1</sub>	0.20 <sup>0.28</sup> <sub>0.12</sub>	0.037 <sup>0.058</sup> <sub>0.016</sub>	0.015 <sup>0.034</sup> <sub>-0.005</sub>
$S_B$ and $\Delta I$ , 45° cutoff	75	13.2 <sup>14.5</sup> <sub>11.8</sub>	0.23 <sup>0.28</sup> <sub>0.18</sub>	0.035 <sup>0.054</sup> <sub>0.015</sub>	0.018 <sup>0.036</sup> <sub>0.001</sub>
$S_B$ and $\Delta I$ , Vandamme cutoff	70	12.4 <sup>13.7</sup> <sub>10.9</sub>	0.23 <sup>0.27</sup> <sub>0.18</sub>	0.032 <sup>0.050</sup> <sub>0.014</sub>	0.012 <sup>0.028</sup> <sub>-0.004</sub>
<b>Matuyama</b>					
$S_B$ and $\Delta I$ , no cutoff	13	15.3 <sup>18.1</sup> <sub>12.6</sub>	0.22 <sup>0.32</sup> <sub>0.13</sub>	0.031 <sup>0.095</sup> <sub>-0.033</sub>	0.020 <sup>0.079</sup> <sub>-0.038</sub>
$S_B$ and $\Delta I$ , 45° cutoff	18	14.7 <sup>17.8</sup> <sub>11.5</sub>	0.22 <sup>0.30</sup> <sub>0.13</sub>	0.019 <sup>0.080</sup> <sub>-0.043</sub>	0.027 <sup>0.081</sup> <sub>-0.027</sub>
$S_B$ and $\Delta I$ , Vandamme cutoff	16	12.1 <sup>15.6</sup> <sub>8.7</sub>	0.24 <sup>0.31</sup> <sub>0.16</sub>	0.036 <sup>0.091</sup> <sub>-0.019</sub>	0.029 <sup>0.077</sup> <sub>-0.018</sub>
<b>Brunhes</b>					
$S_B$ and $\Delta I$ , no cutoff	42	13.3 <sup>15.4</sup> <sub>11.1</sub>	0.18 <sup>0.28</sup> <sub>0.08</sub>	0.020 <sup>0.054</sup> <sub>0.003</sub>	0.017 <sup>0.039</sup> <sub>-0.004</sub>
$S_B$ and $\Delta I$ , 45° cutoff	43	12.4 <sup>14.0</sup> <sub>10.8</sub>	0.20 <sup>0.26</sup> <sub>0.14</sub>	0.031 <sup>0.056</sup> <sub>0.005</sub>	0.018 <sup>0.040</sup> <sub>-0.004</sub>
$S_B$ and $\Delta I$ , Vandamme cutoff	41	11.2 <sup>13.0</sup> <sub>9.5</sub>	0.24 <sup>0.29</sup> <sub>0.18</sub>	0.020 <sup>0.045</sup> <sub>-0.005</sub>	0.013 <sup>0.035</sup> <sub>-0.008</sub>

Note.  $N_{\text{fid}}$  is the number of fitted data to the PSV and TAF models that meet the criterion of Deenen et al. (2011) (see Tables S3–S5). <sup>u</sup>Upper 95% confidence limit. <sub>l</sub>Lower 95% confidence limit.

confidence intervals (Table 1), for instance, the high negative or positive  $\Delta I$  values in Norway (78°N; Cromwell et al., 2013) and Saint Helena Island at 18°S, respectively (Engbers et al., 2020).

$\Delta I$  estimates for the Matuyama chron (Table S4 and Figures 5d–5f) are more limited, with negative and positive values in mid- to high-northern latitudes, while the southern hemisphere has positive (<10°) anomalies; exceptions are low negative  $\Delta I$  values at low latitudes from Ecuador at 0.5°S (Opdyke et al., 2006) and French Polynesia at 18°S (Yamamoto et al., 2002). The distribution of  $\Delta I$  estimates with no VGP cutoff (Figure 5d) is limited, particularly in the southern hemisphere. The best-fit field model yields values of non-dipole contributions  $G_2 = 0.031^{0.095}_{-0.033}$  and  $G_3 = 0.020^{0.079}_{-0.038}$  that are statistically compatible within 95% uncertainty limits compared to parameters obtained for the Matuyama subsets with fixed 45° cutoff ( $G_2 = 0.019^{0.080}_{-0.043}$  and  $G_3 = 0.027^{0.081}_{-0.027}$ , Figure 5e) and Vandamme (1994) cutoff ( $G_2 = 0.036^{0.091}_{-0.019}$  and  $G_3 = 0.029^{0.077}_{-0.018}$ , Figure 5f).

Lastly, the inclination anomaly distribution for Brunhes subsets (Table S5 and Figures 5g–5i) has higher negative (>−5°)  $\Delta I$  values at low southern and northern latitudes. The fitted field model with no VGP cutoff (Figure 5g) has  $G_2 = 0.029^{0.054}_{0.003}$  and  $G_3 = 0.017^{0.039}_{-0.004}$ . Non-dipole zonal terms are statistically identical when transitional data are removed, with  $G_2 = 0.031^{0.056}_{0.005}$ ,  $G_3 = 0.018^{0.039}_{-0.004}$ , and  $G_2 = 0.020^{0.045}_{-0.005}$ ,  $G_3 = 0.013^{0.035}_{-0.008}$  for Brunhes subsets with a fixed 45° cutoff (Figure 5h) and variable cutoff (Figure 5i), respectively.

## 5. Discussion

### 5.1. The New Paleomagnetic Database for 0–10 Ma

Statistical analyses of the latitudinal structure of PSV and TAF were performed for carefully selected paleomagnetic data for the 0–10 Ma period, which provides a high-quality database. About 84% of the new compilation is derived from the PSV10 database of Cromwell et al. (2018). As the primary data source, it is worth mentioning differences between the results obtained by Cromwell et al. (2018) and the present study, particularly regarding data quantity and quality, and the methods used here.

The PSV10 database consists of 2,401 paleodirectional sites from 81 studies. Our data collection increases the number of sites (2,543 records; Table S1), although the number of paleomagnetic studies (80) is a little lower compared to the PSV10 compilation because of the stricter criteria employed here. An improved spatial data distribution is achieved by inclusion of new records from the East Carpathians (Vişan et al., 2016),

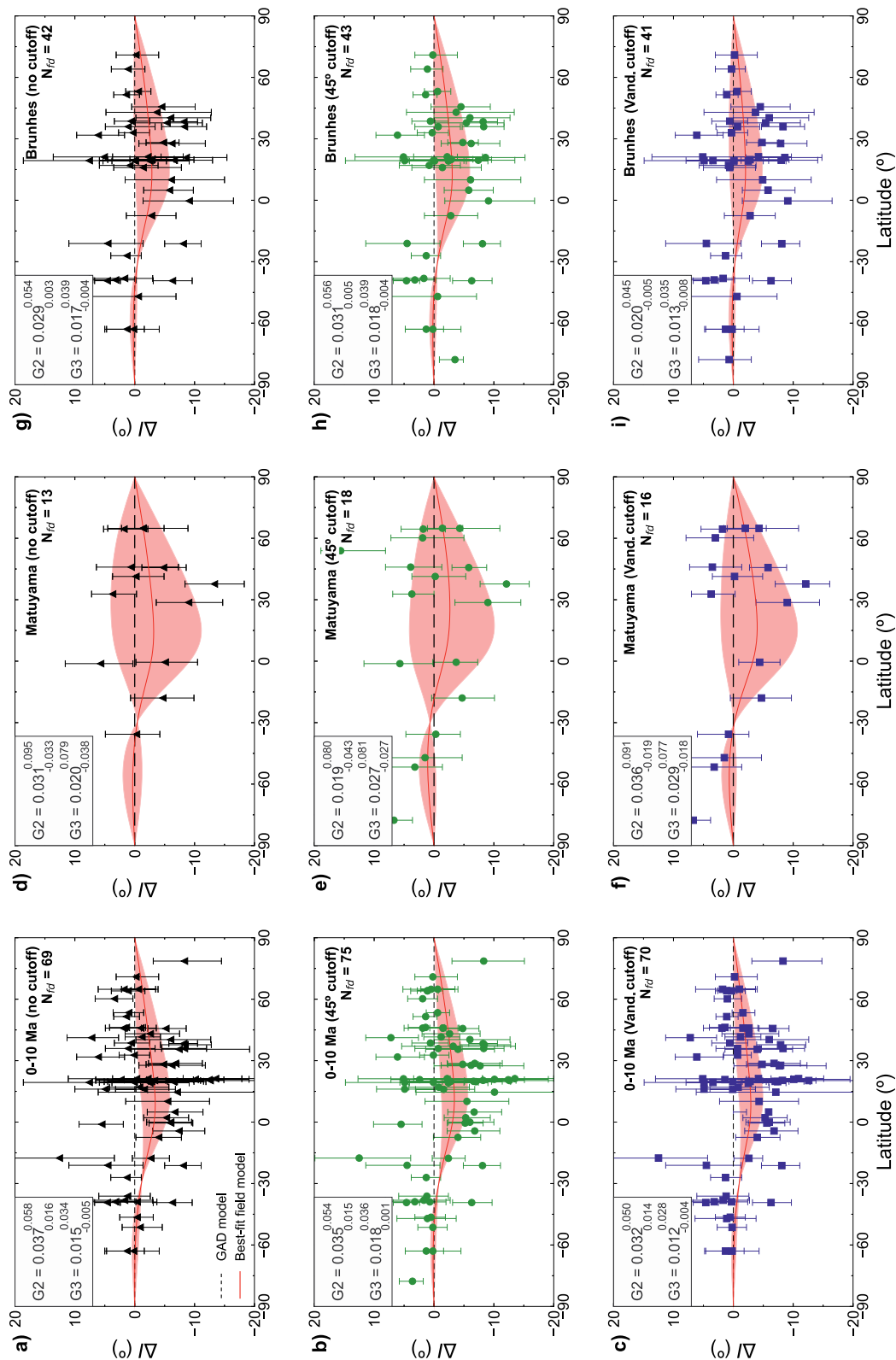


**Figure 5.** Inclination anomaly ( $\Delta I$ ) as a function of latitude defined using three virtual geomagnetic pole cutoff approaches.  $\Delta I$  estimates with 95% bootstrap confidence limits for (a–c) the 0–10 Ma interval, (d–f) Matuyama reverse chron, and (g–i) Brunhes normal chron. Red curves are the best-fit field model for each time period. Red-shaded areas represent the 95% confidence region associated with uncertainties for the zonal quadrupole (G2) and octupole (G3) terms. Each figure includes a GAD field model (black dashed line) at  $\Delta I = 0$ . Vand. = Vandamme (1994).

Israel (Behar et al., 2019), and Saint Helena Island (Engbers et al., 2020). In terms of temporal distribution, there was a 5% increase in data coverage for the age interval older than 5 Ma.

Moreover, our stricter selection criteria incorporate a minimum number of paleodirectional sites per study ( $N \geq 10$ ) and number of samples per site  $n \geq 5$ , which differs from PSV10 database (with  $n \geq 4$ ). These criteria exclude 15 of the original 81 data sets from the PSV10 compilation. Through inspection of the  $S_B$  distribution for individual PSV10 data sets by applying the Vandamme (1994) criterion (hereafter PSV10<sub>vcut</sub>; Table S6), higher  $S_B$  estimates are obtained for some data than are expected from Model G (suggested by Doubrovine et al. [2019]) at mid northern latitudes (Figure S3). Most of these overestimates may be associated with data undersampling, with  $N < 10$ , in accordance with the analyses of J08. Large  $N$  and  $n$  values are recommended to reduce bias in PSV and TAF estimates (Biggin et al., 2008; Johnson & McFadden, 2015). Cromwell et al. (2018) demonstrated that intrasite directional variance is reduced by  $\sim 7\%$  for  $n = 5$  compared to  $n = 4$ . These assessments indicate the high-quality of data sets in the present study that can be used to examine paleofield latitudinal structure.

By comparing the Model G curve fitted to the PSV10<sub>vcut</sub> subset (yellow line in Figure 2d) and the best-fit curve for the new 0–10 Ma data sets using a variable cutoff, a lower latitudinal dependence of the VGP dispersion curve is observed here (Figure 2d). The estimated shape parameter  $a = 12.4^{13.7^\circ}_{10.9}$  is not statistically distinguishable from that for the PSV10<sub>vcut</sub> compilation with  $a = 11.3^{12.6^\circ}_{10.2}$ , and  $b$  also overlaps the 95% confidence intervals ( $b = 0.23^{0.27}_{0.18}$  for the present study and  $b = 0.27^{0.31}_{0.19}$  for PSV10<sub>vcut</sub> subset; Table S7). The small differences in the VGP dispersion curves are probably associated with the method used to estimate PSV. We determined the VGP dispersion for each data set individually, in contrast to the mean  $S_B$  calculated for  $10^\circ$  latitude bands by Cromwell et al. (2018). We choose a statistical approach that allows us to investigate PSV and TAF at the study level, as has been widely employed for studies over the Phanerozoic and Archean time scales (e.g., de Oliveira et al., 2018; Doubrovine et al., 2019; Franco et al., 2019; Veikkolainen & Pesonen, 2014). In addition, it is possible to analyze differences between  $S_B$  estimates that may be caused by the paleomagnetic study location where binning is not viable.

## 5.2. Evidence for Hemispheric Asymmetry of Paleosecular Variation

In order to identify possible VGP dispersions pattern differences between the northern and southern hemispheres, we tested PSV equatorial symmetry by evaluating the latitudinal behavior of the Model G curves fitted to reliable  $S_B$  data for the 0–10 Ma interval (Figure 6a) and Brunhes chron (Figure 6b) for the northern and southern hemispheres (closed and open symbols, respectively). The Matuyama subset was not considered separately due to poor  $S_B$  coverage data over a broad latitudinal range. For the past 10 Myr, the overall patterns of the VGP dispersion curves for the northern and southern hemispheres are similar, regardless of the VGP cutoff filter used (see also Figures S4 and S5 in Supporting Information S1). The best-fit curve for  $S_B$  data using the Vandamme (1994) criterion (Figure 6a) resulted in Model G parameters  $a = 12.4^{14.0^\circ}_{10.7}$  and  $b = 0.23^{0.29}_{0.18}$  for the northern hemisphere, which are statistically indistinguishable at the 95% confidence level compared to the southern hemisphere ( $a = 12.4^{15.1^\circ}_{9.7}$  and  $b = 0.20^{0.31}_{0.09}$ ). Model G curves for  $S_B$  subsets with no VGP cutoff and a  $45^\circ$  cutoff are presented in Figure S4.

For the Brunhes subsets, the best-fit Model G curves suggest northern-southern hemisphere asymmetry. When the variable cutoff is employed (Figure 6b), Model G parameters are  $a = 11.6^{13.6^\circ}_{9.5}$  and  $b = 0.22^{0.30}_{0.14}$  for the northern hemisphere VGP dispersion curve, which are respectively higher and lower than for the southern hemisphere ( $a = 10.7^{14.5^\circ}_{6.9}$  and  $b = 0.25^{0.34}_{0.16}$ ). However, the differences between the Model G parameters are both within the 95% confidence interval (see also Figure S5 for Brunhes subsets without a VGP cutoff and using a constant  $45^\circ$  cutoff).

Based on comparative assessments among VGP dispersion curves for the northern and southern hemispheres for 0–10 Ma and Brunhes data, the latter provides evidence of a hemispheric PSV asymmetry, especially when the Vandamme (1994) criterion is applied. These findings support the hypothesis of higher (lower) VGP dispersion in the southern (northern) hemispheres for at least the past 0.78 Ma. In addition, our quantitative assessment differs from previous observations (Cromwell et al., 2013, 2018). Recent geomagnetic field models that evaluate PSV indices ( $P_p$ , a measure of regional field variability) for present, historical (Panovska & Constable, 2017), multimillennial (0–10 ka; Constable et al. [2016], and 0–100 ka

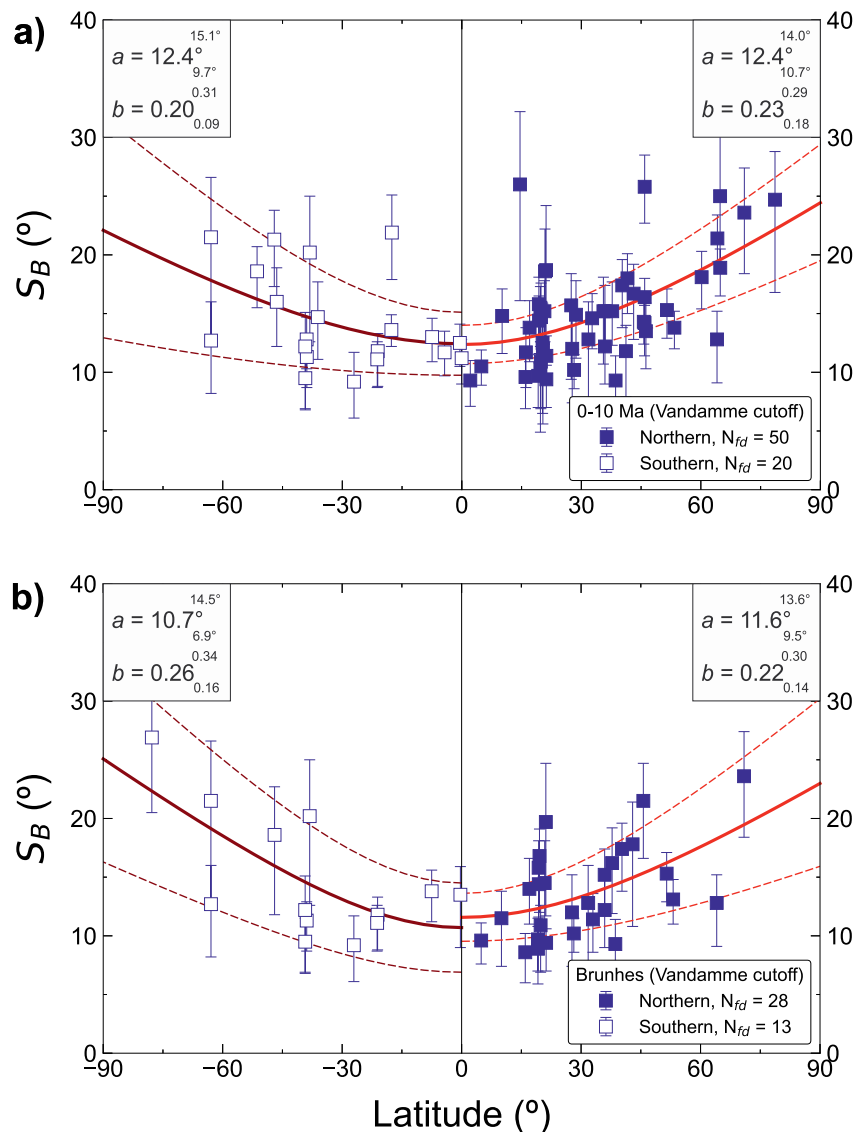


**Figure 6.** Virtual geomagnetic pole dispersion ( $S_B$ ) as a function of latitude for (a) the 0–10 Ma interval and (b) Brunhes chron applying the Vandamme (1994) cutoff. Light (dark) red lines represent the Model G curve fitted to northern (southern) hemisphere data, with its 95% confidence intervals (dashed lines).

[Panovska, Constable, & Brown, 2018; Panovska, Constable, & Korte, 2018]) timescales yield higher  $P_i$  values in the southern hemisphere than the northern hemisphere. These differences are associated with low field intensities, which suggest that the equatorial PSV asymmetry is a long-period feature of the geomagnetic field.

Hemispheric field structure differences have been attributed to lateral CMB heat flux heterogeneity, based on numerical dynamo simulations (e.g., Aubert et al., 2013; Christensen & Olson, 2003; Terra-Nova et al., 2019). Davies et al. (2008) reported a higher latitudinal variation of synthetic VGP dispersion in the southern hemisphere than the north, from a dynamo model run under thermal heterogeneous CMB conditions. However, VGP dispersion estimates observed from the geodynamo models were significantly lower when compared to PSV models (e.g., Johnson et al., 2008; McElhinny & McFadden, 1997).

### 5.3. Comparison With Historical Equivalent VGP Dispersion

It is well known that snapshots of geomagnetic field models are not equivalent to TAF models (Hulot & Gallet, 1996; Kono & Tanaka, 1995; Merrill et al., 1998). Even so, McFadden et al. (1988) showed that VGP dispersion curve for the present geomagnetic field (computed from the IGRF65 model) is similar to the 0–5 Ma paleomagnetic field. Nevertheless, their results only considered the average VGP dispersion over both southern and northern hemispheres. Furthermore, Hulot and Gallet (1996) showed that historical VGP dispersion is highly time-dependent; for earlier historical periods, the similarity observed by McFadden et al. (1988) no longer holds. They also showed that the Gauss coefficients of degree and order (1,1), (2,1), (3,1), and (4,1) are the main terms that influence the shape of the VGP dispersion curve. Here, we further investigate the time dependence of the equatorial asymmetry in VGP scatter curves.

We evaluate the equivalent VGP dispersion for the historical period using the time-dependent geomagnetic field model COV-OBS based on stochastics methods (Gillet et al., 2015). Distributions of dispersion data were computed for each 5° latitude band, with 5° longitude spacing. Equivalent VGP dispersion curves from 1840 to 2015 in five-year intervals are shown in Figure 7a, considering VGP dispersion estimates between northern and southern hemispheres. As expected from previous observations (e.g., McFadden et al., 1988; Hulot & Gallet, 1996), the VGP dispersion tends to increase from the equator to the pole. However, for earlier epochs (before 1880) a decreasing dispersion from 60° latitude is observed. By comparing the Model G best-fit curves from this study with those for previous PSV studies for the 0–5 Ma (Opdyke et al., 2015) and 0–10 Ma (Cromwell et al., 2018) intervals, we detect an incompatibility between paleomagnetic VGP dispersions and equivalent VGP dispersions from a snapshot of historical geomagnetic fields, in contrast to the observations of McFadden et al. (1988). Nevertheless, latitudinal geomagnetic field variation for older periods (yellow curves in Figure 7a) and the 0–10 Ma paleomagnetic field (from this study using the Vandamme [1994] criterion) capture a similar pattern within the 0°–40° latitudinal range.

When historical equivalent VGP dispersions are examined separately for each hemisphere, there is a pronounced equatorial PSV asymmetry especially for recent intervals of geomagnetic field behavior (Figure 7b). Neither the northern nor the southern hemisphere equivalent dispersions have any striking similarity compared to VGP dispersion curves from PSV data (Figure 7a). Southern hemisphere scatter is higher with a bump around 20°, which probably relates to the historical latitudinal position of the South Atlantic Anomaly (e.g., Amit et al., 2021; Hartmann & Pacca, 2009; Terra-Nova et al., 2017). In the northern hemisphere, there is a VGP dispersion decrease with latitude, with a bump at around 50–60°N. A similar feature was found by McFadden et al. (1988) for the IGRF65 model. These results highlight that the historical equivalent VGP dispersions produce higher equatorial asymmetry than that discussed in PSV studies. This could relate to the short time span of the geomagnetic field model, but should not be over-interpreted. Curiously, equivalent southern hemisphere dispersion better describes the paleomagnetic data than the equivalent northern hemisphere dispersion.

We also investigate the spherical harmonics responsible for the observed time evolution of equivalent VGP dispersion curves. First, we calculate dispersion distributions in terms of specific Gauss coefficients from the COV-OBS model for 1965 (Figure 7a). Following Hulot and Gallet (1996), we expand the investigation of how non-zonal harmonic terms of low degree ( $l = 1, 2, 3, 4$ ) and order  $m = 1$  alter the shape of the VGP dispersion curve. The nullifying of certain non-zonal harmonics changes significantly the latitudinal behavior of VGP dispersions. For instance, when the four non-zonal terms are reduced to zero, the dispersion distributions tend to decrease at high latitudes ( $>60^\circ$ ; brown curve in Figure 7c).

To quantify hemispherical differences in the time evolution of historical equivalent VGP dispersions, we define the interhemispheric variance ( $\Delta S$ ) expressed by:

$$\Delta S(\lambda, t) = \sum_0^{\lambda=90} |S_{NH}(\lambda, t) - S_{SH}(-\lambda, t)|, \quad (10)$$

where  $S_{NH}$  and  $S_{SH}$  are dispersion estimates for the northern and southern hemispheres, respectively. The higher  $\Delta S$ , the more asymmetric are the northern and southern equivalent VGP dispersion curves. By evaluating the average energy of non-zonal harmonics as a function of  $\Delta S$  estimates (Figure 7d),  $\Delta S$  is observed to increase progressively with dipole field decay (including the axial  $g_1^0$  term) and increased non-dipole field contributions over historical time. When establishing a linear regression to the data, a best-fit was found for

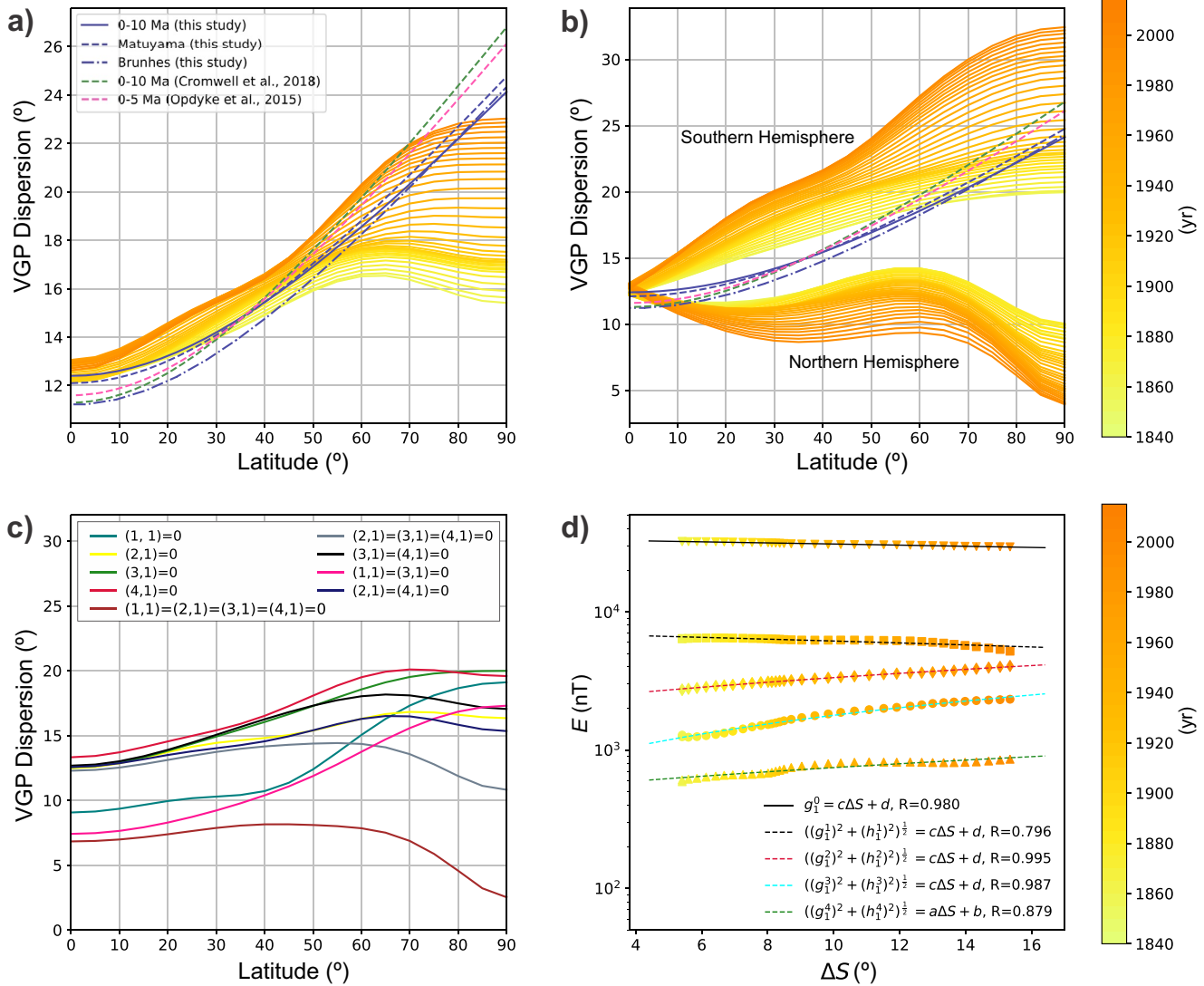


**Figure 7.** Equivalent virtual geomagnetic pole (VGP) dispersion as a function of latitude for the historical period from the COV-OBS field model (a) averaged over both hemispheres, (b) for the northern and southern hemispheres separately. (c) Equivalent VGP dispersion curves defined in terms of the Gauss coefficients filtered from the COV-OBS model for the 1965 epoch. (d) Average spherical harmonics energy as a function of interhemispheric variance ( $\Delta S$ ) from historical VGP dispersions. Solid and dashed lines correspond to linear regressions fitted to  $\Delta S$  estimates defined for the axial dipole term ( $g_1^0$ ) and four non-zonal harmonic terms, respectively.

the (2,1) term. Further investigation of ratios of non-dipolar fields at the CMB might clarify the source of this asymmetry but is beyond the scope of this study.

#### 5.4. Evaluations of Non-Dipole Zonal Terms Over the Last 10 Myr

The new zonal TAF models fitted to  $\Delta I$  data indicate a small non-dipole field contribution. Specifically, for the 0–10 Ma period, the best estimate for the axial quadrupole  $g_2^0$  term is 3.2%–3.7% of  $g_1^0$ , with a smaller axial octupole contribution  $g_3^0$  ranging from 1.2% to 1.8% of  $g_1^0$  (Table 1). Our results suggest that small departures from the GAD model have persisted over long timescales for the 0–100 ka and 0–5 Ma periods. From their GGF100k model (Global Geomagnetic Field for the 0–100 ka interval), Panovska, Constable, and Korte (2018) revealed the presence of the zonal terms  $G_2 = 4.2\%$  and  $G_3 = 2.5\%$ . For a statistical TAF model for the last 5 Myr, J08 suggests estimates of  $G_2 = 3\%$  and  $G_3 = 3\%$  from high-quality paleomagnetic data. From the PSV10 compilation, Cromwell et al. (2018) estimated axial quadrupole and octupole contributions

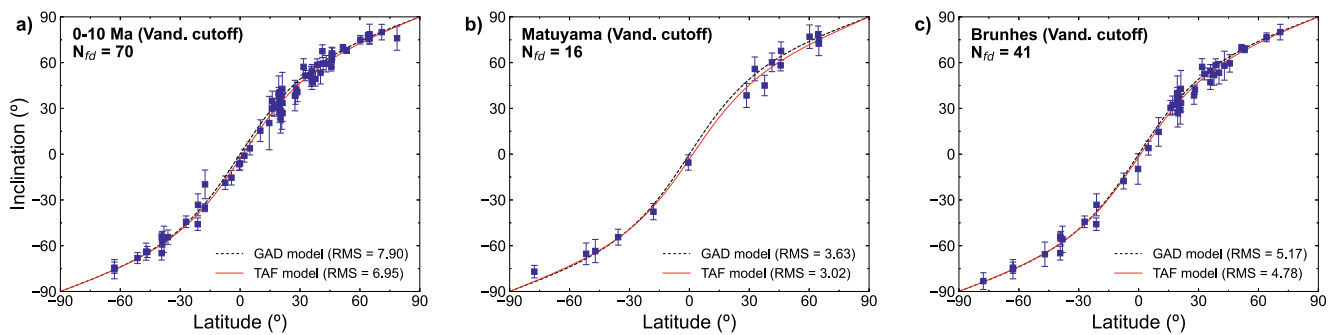


**Figure 8.** Mean inclination as a function of latitude for (a) 0–10 Ma interval, (b) Matuyama chron, and (c) Brunhes chron applying the Vandamme (1994) criterion. The uncertainties of the inclination data correspond to the 95% confidence cone ( $\alpha_{95}$ ) of the mean direction. Black curves represent the expected GAD inclination. Red curves are the inclination predicted for TAF models proposed in this study (see Table 1). Vand. = Vandamme (1994); RMS = root mean square.

of  $g_2^0 = 3\%$  of  $g_1^0$  and  $g_3^0 = 1.3\%$  of  $g_1^0$ , respectively. The BB18.Z3 model (Bono et al., 2020) suggests values of  $G2 = 2.9\%$  and  $G3 = -1.3\%$  for the past 10 Myr. Thus, small non-GAD contributions seem to be a common feature of paleomagnetic field models.

### 5.5. Examining Paleomagnetic Inclinations Relative to the GAD Approximation

The question of the paleomagnetic field geometry found to be predominantly dipolar over the past million years has been debated (Johnson & McFadden, 2015; McElhinny, 2004). For the three time periods investigated in this study, our TAF models reveal low values of the  $G2$  and  $G3$  terms (Table 1). Following the previous TAF studies (e.g., Opdyke & Henry, 1969; Opdyke et al., 2015; Schneider & Kent, 1990), we also examine the latitudinal distribution of mean inclination data (applying the Vandamme [1994] cutoff) to test compliance with the expected GAD inclination (determined by Equation 7), as shown in Figure 8.

Most of mean inclination data for the 0–10 Ma interval agree with the latitudinal variation curve from a GAD model (black dashed line in Figure 8a), and are not statistically different at the 95% confidence level relative to predicted GAD inclination. Similarly, Matuyama reverse and Brunhes normal polarity data (Figures 8b and 8c, respectively) show a close correspondence with the GAD inclination curve, considering the 95% uncertainties of the mean inclinations. Nevertheless, the Matuyama estimates at northern latitudes produce large deviations from the GAD prediction compared to the Brunhes chron.

For each age group, we calculate the weighted root mean square (RMS) deviation of the difference between the mean paleomagnetic inclination and the predicted GAD inclination. The weights correspond to the 95% uncertainties of the mean paleomagnetic direction. Our analyses show that the three temporal data sets are best-fit for the corresponding TAF models presented in this study (summarized in Table 1), with slightly lower RMS values than for GAD model. The inclination curves for TAF models (red line) are shown in Figure 8. These results suggest that the inclination estimates are compatible with the GAD field, however, the paleofield models with small  $G2$  and  $G3$  contributions provide a statistically acceptable fit to the observed inclination data. Furthermore, the non-dipole field components do not yield significant changes for the last 10 Myr.

### 5.6. Distinct PSV and TAF Patterns: Brunhes Normal and Matuyama Reverse Polarity Data Sets

Statistical analysis of PSV and TAF latitudinal behavior reveals differences between the Brunhes normal and Matuyama reverse polarity data, which partially supports the observations of J08. For PSV analysis, we examine Model G parameter estimates fitted to  $S_B$  data for both age groups, which differs from that presented by J08. Best-fit curves for Matuyama subsets yield higher  $S_B$  estimates at low latitudes compared to the Brunhes subsets, especially when a  $45^\circ$  cutoff angle is used to exclude outlier data (Figures 3 and 4). When compared to J08, our Matuyama estimates (using a fixed  $45^\circ$  cutoff) produce less latitudinal variation in the VGP dispersion curve (Figure 3c). However, the difference is statistically significant with respect to Model G parameter  $b$  (Table 1 and Table S7). Differences between the two VGP dispersion curves are probably

related to inclusion of new mid- to high-latitude ( $\pm 50\text{--}65^\circ$ ) records that were not included in J08 and that may have influenced the Model G fit. For the Brunhes chron (Figure 4c), our predicted  $S_B$  values for Model G are lower for J08, but Model G parameters in both studies are not statistically distinguishable at the 95% confidence level. The slight observed differences may be associated with the data sets distribution and size in both studies (Table 1 and Table S7).

According to some studies (Cromwell et al., 2018; Valet & Herrero-Bervera, 2011), high (low)  $S_B$  estimates for reverse (normal) polarity fields might be attributed to lower (higher) average paleointensity during the Matuyama (Brunhes) chron. Ahn and Yamamoto (2019) analyzed 0–5 Ma absolute paleointensity data from the PINT database (Biggin et al., 2009) and concluded that the Matuyama had a lower dipole field strength compared to the Brunhes period. Recent studies (Biggin et al., 2020; Meduri et al., 2021) have also pointed out an inverse relationship between the  $a$  parameter from Model G with the degree of dipole dominance, inferred from numerical geodynamo models. Here, the shape parameter  $a$  is higher for Matuyama data sets than for the Brunhes, whichever VGP cutoff is applied (Table 1). These findings suggest that the TAF was less dipolar during the Matuyama than the Brunhes chron. However, observed differences between Model G parameters for these two age groups are not statistically significant at the 95% confidence level.

Zonal TAF model fits for the Matuyama  $\Delta I$  data result in higher quadrupole (G2 of 3.1%–3.6%) and octupole (G3 of 2.0%–2.9%) contributions compared to Brunhes estimates (G2 = 2.0–3.1% and G3 = 1.3–1.8%). The exception is the low value obtained for the G2 term by applying a fixed  $45^\circ$  cutoff (see Table 1). J08 reported estimates of G2 = 4% and G3 = 5% and G2 = 2% and G3 = 1% for the Matuyama and Brunhes chrons, respectively. The main differences in TAF estimates between the studies can be assigned to two factors: (a) incorporation of new data produced after J08 and (b) the formalism used for  $\Delta I$  calculations (here  $\Delta I$  estimates were calculated for each paleomagnetic study instead of latitude band averages, as adopted by J08). Furthermore, high estimates of non-dipole components detected for the Matuyama epoch could be linked to the lower dipolar paleofield dominance in this period than during the Brunhes chron.

Thermal and compositional heterogeneities at the CMB have been suggested as a possible explanation for differences between normal and reverse polarity fields, as debated in the literature (Johnson & McFadden, 2015). McElhinny and McFadden (1997) suggested that distinctions between these two polarity states, ascertained from the latitudinal behavior of 0–5 Ma VGP dispersions, could rather be caused by incompletely removed viscous overprints for reverse polarity data (with higher dispersion compared to normal polarity data). However, considering the high-quality data assessed in this study, we assume that this effect is minimized. Thus, polarity asymmetries in the PSV and TAF models for Matuyama and Brunhes subsets appear to be an empirical feature of the paleomagnetic field, which corroborate earlier observations (e.g., Cromwell et al., 2018; Johnson et al., 2008).

## 6. Conclusions

1. An upgraded database of high-quality igneous paleodirections produced using rigorous selection criteria, provides robust PSV and TAF assessments for the Brunhes and Matuyama chrons over the 0–10 Ma period. The new data compilation contains 2,543 paleomagnetic sites covering the past 10 Myr, which improves the temporal and spatial distributions of paleodirectional data relative to the previous PSV10 database (Cromwell et al., 2018).
2. VGP dispersion patterns from the 0–10 Ma data set, and from Matuyama and Brunhes subsets, are well-fitted by an adapted Model G (McFadden et al., 1988) that differs slightly from the dispersions predicted by the GGP models BCE19 (Brandt et al., 2020) and BB18 and BB18.Z3 (Bono et al., 2020). It is noteworthy that the BCE19 model and BB18-family models were designed to fit, respectively, paleodirectional and VGP dispersion estimates in the PSV10 compilation.
3. The VGP dispersion curve fitted for new 0–10 Ma data sets using Model G produces lower latitudinal dependence of  $S_B$  than the PSV10 data set. Analyses of the  $S_B$  data as a function of latitude suggest that differences in the shape of Model G curves are associated with data selection and calculation methods for PSV estimates. Our results differ by including more stringent quality criteria (with  $N \geq 10$ ,  $n \geq 5$ ), and assess latitudinal PSV variation by locality using the Deenen et al. (2011) criterion rather than mean  $S_B$  values by latitude bands.

4. New zonal TAF model for the 0–10 Ma interval indicate the presence of small non-dipole field contributions, with an axial quadrupole component  $G_2 = 3.2\text{--}3.7\%$  and a smaller axial octupole component  $G_3 = 1.2\text{--}1.8\%$ .
5. Assessments of the latitudinal PSV behavior do not provide clear evidence of a north-south hemispheric asymmetry in VGP dispersion for 0–10 Ma data sets. Brunhes data have differences between hemispheres that are characterized by a stronger latitudinal  $S_B$  dependence in the southern relative to the northern hemisphere, especially when the Vandamme (1994) cutoff is used. This finding suggest that equatorial asymmetry of geomagnetic secular variation has persisted over the last 780 ka.
6. Statistical simulations from the COV-OBS model for the 1965 epoch indicate that the reduction or combined effect of non-zonal harmonic terms (1,1), (2,1), (3,1), and (4,1) to zero implies significant modifications in the shape of the equivalent VGP dispersion curve. Furthermore, investigations of the historical evolution of dispersion estimates for the northern and southern hemispheres indicate an equatorial asymmetry of VGP scatter that gradually increases with time, which can be associated with dipole field decay and increased non-dipole field contributions.
7. We report differences between Brunhes normal and Matuyama reverse polarity data in both PSV and the TAF analysis. The Matuyama subset produces higher  $S_B$  patterns at low latitudes than the Brunhes chron. In terms of non-GAD TAF structure, zonal quadrupole and octupole contributions are larger for the Matuyama chron (with  $G_2 = 3.1\text{--}3.6\%$  and  $G_3 = 2.0\text{--}2.9\%$ ) compared to the Brunhes ( $G_2 = 2.0\text{--}3.1\%$  and  $G_3 = 1.3\text{--}1.8\%$ ), which support observations of lower and higher average paleointensities for the respective periods.
8. Finally, additional high-quality data are essential to enhance temporal and geographic sampling of the 0–10 Ma database (especially data coverage older than 1 Ma and new southern hemisphere records), and to better understand long-period geomagnetic field asymmetries.

## Data Availability Statement

Tables S2–S6 are available at the Earth Reference Digital Archive (<http://earthref.org/ERDA/2476/>).

## Acknowledgments

The authors acknowledge the comments and suggestions of A. Roberts and an anonymous reviewer, and the editorial work of J. Feinberg. This work was supported by grants from the Conselho Nacional de Desenvolvimento Científico e Tecnológico (CNPq, #165161/2018-3, #425728/2018-8, #312737/2020-3). A. J. Biggin and Y. A. Engbers acknowledge support from The Leverhulme Trust (RLA-2016-080), and R. K. Bono acknowledges support from The Leverhulme Trust (ECF-2020-617).

## References

- Ahn, H. S., & Yamamoto, Y. (2019). Paleomagnetic study of basaltic rocks from Baengnyeong Island, Korea: Efficiency of the Tsunakawa–Shaw paleointensity determination on non-SD-bearing materials and implication for the early Pliocene geomagnetic field intensity. *Earth, Planets and Space*, 71(1), 126. <https://doi.org/10.1186/s40623-019-1107-6>
- Amit, H., Terra-Nova, F., Lézin, M., & Trindade, R. I. (2021). Non-monotonic growth and motion of the South Atlantic Anomaly. *Earth, Planets and Space*, 73(1), 1–10. <https://doi.org/10.1186/s40623-021-01356-w>
- Argus, D. F., Gordon, R. G., & DeMets, C. (2011). Geologically current motion of 56 plates relative to the no-net-rotation reference frame. *Geochemistry, Geophysics, Geosystems*, 12(11). <https://doi.org/10.1029/2011GC003751>
- Aster, R. C., Borchers, B., & Thurber, C. H. (2012). *Parameter estimation and inverse problems*. Elsevier.
- Aubert, J., Finlay, C. C., & Fournier, A. (2013). Bottom-up control of geomagnetic secular variation by the Earth's inner core. *Nature*, 502(7470), 219–223. <https://doi.org/10.1038/nature12574>
- Aubert, J., Tarduno, J. A., & Johnson, C. L. (2010). Observations and models of the long-term evolution of Earth's magnetic field. *Space Science Reviews*, 155(1–4), 337–370. <https://doi.org/10.1007/s11214-010-9684-5>
- Behar, N., Shaar, R., Tauxe, L., Asefaw, H., Ebert, Y., Heimann, A., et al. (2019). Paleomagnetism and paleosecular variations from the Plio-Pleistocene Golan Heights volcanic plateau, Israel. *Geochemistry, Geophysics, Geosystems*, 20(9), 4319–4335. <https://doi.org/10.1029/2019GC008479>
- Biggin, A., Bono, R., Meduri, D. G., Sprain, C., Davies, C. J., Holme, R., & Doubrovine, P. (2020). Quantitative estimates of average geomagnetic axial dipole dominance in deep geological time. *Nature Communications*, 11(1), 1–9. <https://doi.org/10.1038/s41467-020-19794-7>
- Biggin, A. J., Strik, G. H. M. A., & Langereis, C. G. (2009). The intensity of the geomagnetic field in the late-Archaeon: New measurements and an analysis of the updated IAGA palaeointensity database. *Earth, Planets and Space*, 61(1), 9–22. <https://doi.org/10.1186/BF03352881>
- Biggin, A. J., Van Hinsbergen, D. J., Langereis, C. G., Straathof, G. B., & Deenen, M. H. (2008). Geomagnetic secular variation in the Cretaceous Normal Superchron and in the Jurassic. *Physics of the Earth and Planetary Interiors*, 169(1–4), 3–19. <https://doi.org/10.1016/j.pepi.2008.07.004>
- Bono, R. K., Biggin, A. J., Holme, R., Davies, C. J., Meduri, D. G., & Bestard, J. (2020). Covariant giant Gaussian process models with improved reproduction of palaeosecular variation. *Geochemistry, Geophysics, Geosystems*, 21(8). <https://doi.org/10.1029/2020GC008960>
- Brandt, D., Constable, C., & Ernesto, M. (2020). Giant Gaussian process models of geomagnetic paleosecular variation: A directional outlook. *Geophysical Journal International*, 22(3), 1526–1541. <https://doi.org/10.1093/gji/ggaa258>
- Christensen, U. R., & Olson, P. (2003). Secular variation in numerical geodynamo models with lateral variations of boundary heat flow. *Physics of the Earth and Planetary Interiors*, 138(1), 39–54. [https://doi.org/10.1016/S0031-9201\(03\)00064-5](https://doi.org/10.1016/S0031-9201(03)00064-5)
- Coe, R. S., & Glatzmaier, G. A. (2006). Symmetry and stability of the geomagnetic field. *Geophysical Research Letters*, 33(21). <https://doi.org/10.1029/2006GL027903>

- Constable, C., Korte, M., & Panovska, S. (2016). Persistent high paleosecular variation activity in southern hemisphere for at least 10 000 years. *Earth and Planetary Science Letters*, 453, 78–86. <https://doi.org/10.1016/j.epsl.2016.08.015>
- Constable, C. G., & Johnson, C. L. (1999). Anisotropic paleosecular variation models: Implications for geomagnetic field observables. *Physics of the Earth and Planetary Interiors*, 115(1), 35–51. [https://doi.org/10.1016/S0031-9201\(99\)00065-5](https://doi.org/10.1016/S0031-9201(99)00065-5)
- Constable, C. G., & Parker, R. L. (1988). Statistics of the geomagnetic secular variation for the past 5 m.y. *Journal of Geophysical Research*, 93(B10), 11569–11581. <https://doi.org/10.1029/JB093iB10p11569>
- Cox, A. (1970). Latitude dependence of the angular dispersion of the geomagnetic field. *Geophysical Journal of the Royal Astronomical Society*, 20(3), 253–269. <https://doi.org/10.1111/j.1365-246X.1970.tb06069.x>
- Cox, A. (1975). The frequency of geomagnetic reversals and the symmetry of the nondipole field. *Reviews of Geophysics*, 13(3), 35–51. <https://doi.org/10.1029/RG013i003p00035>
- Cromwell, G., Johnson, C. L., Tauxe, L., Constable, C. G., & Jarboe, N. A. (2018). PSV10: A global data set for 0–10 Ma time-averaged field and paleosecular variation studies. *Geochemistry, Geophysics, Geosystems*, 19(5), 1533–1558. <https://doi.org/10.1002/2017GC007318>
- Cromwell, G., Tauxe, L., Staudigel, H., Constable, C. G., Koppers, A. A. P., & Pedersen, R. B. (2013). In search of long-term hemispheric asymmetry in the geomagnetic field: Results from high northern latitudes. *Geochemistry, Geophysics, Geosystems*, 14(8), 3234–3249. <https://doi.org/10.1002/ggge.20174>
- Davies, C. J., Gubbins, D., Willis, A. P., & Jimack, P. K. (2008). Time-averaged paleomagnetic field and secular variation: Predictions from dynamo solutions based on lower mantle seismic tomography. *Physics of the Earth and Planetary Interiors*, 169(1–4), 194–203. <https://doi.org/10.1016/j.pepi.2008.07.021>
- Deenen, M. H., Langereis, C. G., van Hinsbergen, D. J., & Biggin, A. J. (2011). Geomagnetic secular variation and the statistics of palaeomagnetic directions. *Geophysical Journal International*, 186(2), 509–520. <https://doi.org/10.1111/j.1365-246X.2011.05050.x>
- de Oliveira, W. P., Franco, D. R., Brandt, D., Ernesto, M., da Ponte Neto, C. F., Zhao, X., et al. (2018). Behavior of the paleosecular variation during the Permian–Carboniferous reversed Superchron and comparisons to the low reversal frequency intervals since Precambrian times. *Geochemistry, Geophysics, Geosystems*, 19(4), 1035–1048. <https://doi.org/10.1002/2017GC007262>
- Dobrovine, P. V., Veikkola, T., Pesonen, L. J., Piispa, E., Ots, S., Smirnov, A. V., et al. (2019). Latitude dependence of geomagnetic paleosecular variation and its relation to the frequency of magnetic reversals: Observations from the Cretaceous and Jurassic. *Geochemistry, Geophysics, Geosystems*, 20(3), 1240–1279. <https://doi.org/10.1029/2018GC007863>
- Efron, B., & Tibshirani, R. (1993). *An introduction to the bootstrap*. Chapman & Hall.
- Engbers, Y. A., Biggin, A. J., & Bono, R. K. (2020). Elevated paleomagnetic dispersion at Saint Helena suggests long-lived anomalous behavior in the South Atlantic. *Proceedings of the National Academy of Sciences*, 117(31), 18258–18263. <https://doi.org/10.1073/pnas.2001217117>
- Fisher, R. A. (1953). Dispersion on a sphere. *Proceedings of the Royal Society of London A*, 217(1130), 295–305. <https://doi.org/10.1098/rspa.1953.0064>
- Franco, D. R., de Oliveira, W. P., de Freitas, F. B. V., Takahashi, D., da Ponte Neto, C. F., & Peixoto, I. M. C. (2019). Paleomagnetic evidence for inverse correspondence between the relative contribution of the axial dipole field and CMB heat flux for the past 270 Myr. *Scientific Reports*, 9(1), 1–8. <https://doi.org/10.1038/s41598-018-36494-x>
- Gillet, N., Barrois, O., & Finlay, C. C. (2015). Stochastic forecasting of the geomagnetic field from the COV-OBS.x1 geomagnetic field model, and candidate models for IGRF-12. *Earth, Planets and Space*, 67(1), 1–14. <https://doi.org/10.1186/s40623-015-0225-z>
- Hartmann, G. A., & Pacca, I. G. (2009). Time evolution of the South Atlantic magnetic anomaly. *Anais da Academia Brasileira de Ciências*, 81(2), 243–255. <https://doi.org/10.1590/S0001-37652009000200010>
- Hulot, G., Finlay, C. C., Constable, C. G., Olsen, N., & Manda, M. (2010). The magnetic field of planet Earth. *Space Science Reviews*, 152(1), 159–222. <https://doi.org/10.1007/s11214-010-9644-0>
- Hulot, G., & Gallet, Y. (1996). On the interpretation of virtual geomagnetic pole (VGP) scatter curves. *Physics of the Earth and Planetary Interiors*, 95(1–2), 37–53. [https://doi.org/10.1016/0031-9201\(95\)03106-5](https://doi.org/10.1016/0031-9201(95)03106-5)
- Johnson, C. L., Constable, C. G., Tauxe, L., Barendregt, R., Brown, L. L., Coe, R. S., et al. (2008). Recent investigations of the 0–5 Ma geomagnetic field recorded by lava flows. *Geochemistry, Geophysics, Geosystems*, 9(4). <https://doi.org/10.1029/2007GC001696>
- Johnson, C. L., & McFadden, P. L. (2015). The time-averaged field and paleosecular variation. In M. Kono & G. Schubert (Eds.), *Geomagnetism. Treatise on geophysics* (2nd ed., Vol. 5, pp. 385–417). Elsevier. <https://doi.org/10.1016/b978-0-444-53802-4.00105-6>
- Kono, M., & Tanaka, H. (1995). Mapping the Gauss coefficients to the pole and the models of paleosecular variation. *Journal of Geomagnetism and Geoelectricity*, 47(1), 115–130. <https://doi.org/10.5636/jgg.47.115>
- Lawrence, K. P., Tauxe, L., Staudigel, H., Constable, C. G., Koppers, A., McIntosh, W., & Johnson, C. L. (2009). Paleomagnetic field properties at high southern latitude. *Geochemistry, Geophysics, Geosystems*, 10(1). <https://doi.org/10.1029/2008GC002072>
- Lee, S. (1983). *A study of the time-averaged paleomagnetic field for the past 195 million years* (Ph.D. thesis). Australian National University.
- Lhuillier, F., Shcherbakov, V. P., Gilder, S. A., & Hagstrum, J. T. (2017). Variability of the 0–3 Ma paleomagnetic field observed from the Boring Volcanic Field of the Pacific Northwest. *Geophysical Journal International*, 211(1), 69–79. <https://doi.org/10.1093/gji/ggx288>
- Lowes, F. J. (1974). Spatial power spectrum of the main geomagnetic field, and extrapolation to the core. *Geophysical Journal International*, 36(3), 717–730. <https://doi.org/10.1111/j.1365-246X.1974.tb00622.x>
- McElhinny, M. (2004). *Geocentric axial dipole hypothesis: A least squares perspective* Vol. (145, pp. 1–12). American Geophysical Union Geophysical Monograph Series. <https://doi.org/10.1029/145GM01>
- McElhinny, M. W., & McFadden, P. L. (1997). Palaeosecular variation over the past 5 Myr based on a new generalized database. *Geophysical Journal International*, 131(2), 240–252. <https://doi.org/10.1111/j.1365-246X.1997.tb01219.x>
- McElhinny, M. W., & McFadden, P. L. (2000). *Paleomagnetism: Continents and oceans*. Academic Press.
- McElhinny, M. W., McFadden, P. L., & Merrill, R. T. (1996). The time-averaged paleomagnetic field 0–5 Ma. *Journal of Geophysical Research*, 101(B11), 25007–25027. <https://doi.org/10.1029/96JB01911>
- McElhinny, M. W., & Merrill, R. T. (1975). Geomagnetic secular variation over the past 5 m.y. *Reviews of Geophysics and Space Physics*, 13(5), 687–708. <https://doi.org/10.1029/RG013i005p00687>
- McFadden, P. L., Merrill, R. T., & McElhinny, M. W. (1988). Dipole/quadrupole family modeling of paleosecular variation. *Journal of Geophysical Research*, 93(B10), 11583–11588. <https://doi.org/10.1029/JB093iB10p11583>
- Meduri, D. G., Biggin, A. J., Davies, C. J., Bono, R. K., Sprain, C. J., & Wicht, J. (2021). Numerical dynamo simulations reproduce palaeomagnetic field behaviour. *Geophysical Research Letters*, 48(5). <https://doi.org/10.1029/2020GL090544>
- Merrill, R. T., & McElhinny, M. W. (1977). Anomalies in the time-averaged paleomagnetic field and their implications for the lower mantle. *Reviews of Geophysics*, 15(3), 309–323. <https://doi.org/10.1029/RG015i003p00309>

- Merrill, R. T., McElhinny, M. W., & McFadden, P. L. (1998). The magnetic field of the Earth: Paleomagnetism, the core, and the deep mantle. In *International Geophysics Series* Vol. (63). Academic Press.
- Merrill, R. T., & McFadden, P. L. (2003). The geomagnetic axial dipole field assumption. *Physics of the Earth and Planetary Interiors*, 139(3–4), 171–185. <https://doi.org/10.1016/j.pepi.2003.07.016>
- Merrill, R. T., McFadden, P. L., & McElhinny, M. W. (1990). Paleomagnetic tomography of the core-mantle boundary. *Physics of the Earth and Planetary Interiors*, 64(1), 87–101. [https://doi.org/10.1016/0031-9201\(90\)90007-K](https://doi.org/10.1016/0031-9201(90)90007-K)
- Opdyke, N. D., Hall, M., Mejia, V., Huang, K., & Foster, D. A. (2006). Time-averaged field at the equator: Results from Ecuador. *Geochemistry, Geophysics, Geosystems*, 7(11). <https://doi.org/10.1029/2005GC001221>
- Opdyke, N. D., & Henry, K. W. (1969). A test of the dipole hypothesis. *Earth and Planetary Science Letters*, 6(2), 139–151. [https://doi.org/10.1016/0012-821X\(69\)90132-0](https://doi.org/10.1016/0012-821X(69)90132-0)
- Opdyke, N. D., Kent, D. V., Foster, D. A., & Huang, K. (2015). Paleomagnetism of Miocene volcanics on Sao Tome: Paleosecular variation at the Equator and a comparison to its latitudinal dependence over the last 5 Myr. *Geochemistry, Geophysics, Geosystems*, 16(11), 3870–3882. <https://doi.org/10.1002/2015GC005901>
- Panovska, S., & Constable, C. G. (2017). An activity index for geomagnetic paleosecular variation, excursions, and reversals. *Geochemistry, Geophysics, Geosystems*, 18(4), 1366–1375. <https://doi.org/10.1002/2016GC006668>
- Panovska, S., Constable, C. G., & Brown, M. C. (2018). Global and regional assessments of paleosecular variation activity over the past 100 ka. *Geochemistry, Geophysics, Geosystems*, 19(5), 1559–1580. <https://doi.org/10.1029/2017GC007271>
- Panovska, S., Constable, C. G., & Korte, M. (2018). Extending global continuous geomagnetic field reconstructions on timescales beyond human civilization. *Geochemistry, Geophysics, Geosystems*, 19(12), 4757–4772. <https://doi.org/10.1029/2018GC007966>
- Quidelleur, X., & Courtillot, V. (1996). On low-degree spherical harmonic models of paleosecular variation. *Physics of the Earth and Planetary Interiors*, 95(1–2), 55–77. [https://doi.org/10.1016/0031-9201\(95\)03115-4](https://doi.org/10.1016/0031-9201(95)03115-4)
- Schneider, D. A., & Kent, D. V. (1990). The time-averaged paleomagnetic field. *Reviews of Geophysics*, 28(1), 71–96. <https://doi.org/10.1029/RG028i001p00071>
- Sprain, C. J., Biggin, A. J., Davies, C. J., Bono, R. K., & Meduri, D. G. (2019). An assessment of long duration geodynamo simulations using new paleomagnetic modeling criteria (QPM). *Earth and Planetary Science Letters*, 526, 115758. <https://doi.org/10.1016/j.epsl.2019.115758>
- Tauxe, L., & Kent, D. V. (2004). A simplified statistical model for the geomagnetic field and the detection of shallow bias in paleomagnetic inclinations: Was the ancient magnetic field dipolar? In J. E. T. Channell, D. V. Kent, W. Lowrie, & J. G. Meert (Eds.), *Timescales of the paleomagnetic field* (pp. 101–115). American Geophysical Union. <https://doi.org/10.1029/145GM08>
- Tauxe, L., Shaar, R., Jonestrask, L., Swanson-Hysell, N. L., Minnett, R., Koppers, A. A. P., et al. (2016). PmagPy: Software package for paleomagnetic data analysis and a bridge to the Magnetics Information Consortium (MagIC) Database. *Geochemistry, Geophysics, Geosystems*, 17(6), 2450–2463. <https://doi.org/10.1002/2016GC006307>
- Terra-Nova, F., Amit, H., & Choblet, G. (2019). Preferred locations of weak surface field in numerical dynamos with heterogeneous core–mantle boundary heat flux: Consequences for the South Atlantic Anomaly. *Geophysical Journal International*, 217(2), 1179–1199. <https://doi.org/10.1093/gji/ggy519>
- Terra-Nova, F., Amit, H., Hartmann, G. A., Trindade, R. I., & Pinheiro, K. J. (2017). Relating the South Atlantic Anomaly and geomagnetic flux patches. *Physics of the Earth and Planetary Interiors*, 266, 39–53. <https://doi.org/10.1016/j.pepi.2017.03.002>
- Valet, J. P., & Herrero-Bervera, E. (2011). Time-averaged and mean axial dipole field. In *The Earth's magnetic interior* Vol. (1, pp. 131–137). Springer. [https://doi.org/10.1007/978-94-007-0323-0\\_9](https://doi.org/10.1007/978-94-007-0323-0_9)
- Vandamme, D. (1994). A new method to determine paleosecular variation. *Physics of the Earth and Planetary Interiors*, 85(1–2), 131–142. [https://doi.org/10.1016/0031-9201\(94\)90012-4](https://doi.org/10.1016/0031-9201(94)90012-4)
- Veikkolainen, T., & Pesonen, L. J. (2014). Palaeosecular variation, field reversals and the stability of the geodynamo in the Precambrian. *Geophysical Journal International*, 199(3), 1515–1526. <https://doi.org/10.1093/gji/ggu348>
- Vişan, M., Panaiotu, C. G., Necula, C., & Dumitru, A. (2016). Palaeomagnetism of the Upper Miocene-Lower Pliocene lavas from the East Carpathians: Contribution to the paleosecular variation of geomagnetic field. *Scientific Reports*, 6, 23411. <https://doi.org/10.1038/srep23411>
- Yamamoto, Y., Shimura, K., Tsunakawa, H., Kogiso, T., Uto, K., Oda, H., et al. (2002). Geomagnetic paleosecular variation for the past 5 Ma in the Society Islands, French Polynesia. *Earth, Planets and Space*, 54(7), 797–802. <https://doi.org/10.1186/BF03351733>

## References From the Supporting Information

- Alva-Valdivia, L. M. (2005). Comprehensive paleomagnetic study of a succession of Holocene olivine-basalt flow: Xitle Volcano (Mexico) revisited. *Earth, Planets and Space*, 57(9), 839–853. <https://doi.org/10.1186/BF03351862>
- Baraldo, A., Rapalini, A. E., Böhnell, H., & Mena, M. (2003). Paleomagnetic study of Deception Island, South Shetland Islands, Antarctica. *Geophysical Journal International*, 153(2), 333–343. <https://doi.org/10.1046/j.1365-246X.2003.01881.x>
- Brown, L. L., Singer, B. S., & Gorrying, M. L. (2004). Paleomagnetism and <sup>40</sup>Ar/<sup>39</sup>Ar chronology of lavas from Meseta del Lago Buenos Aires, Patagonia. *Geochemistry, Geophysics, Geosystems*, 5(1). <https://doi.org/10.1029/2003GC000526>
- Brown, M. C., Singer, B. S., Knudsen, M. F., Jicha, B. R., Finnes, E., & Feinberg, J. M. (2009). No evidence for Brunhes age excursions, Santo Antão, Cape Verde. *Earth and Planetary Science Letters*, 287(1–2), 100–115. <https://doi.org/10.1016/j.epsl.2009.07.039>
- Calvo-Rathert, M., Goguitchaichvili, A., Bógalo, M. F., Vegas-Tubía, N., Carrancho, Á., & Sologashvili, J. (2011). A paleomagnetic and paleointensity study on Pleistocene and Pliocene basaltic flows from the Djavakheti Highland (Southern Georgia, Caucasus). *Physics of the Earth and Planetary Interiors*, 187(3–4), 212–224. <https://doi.org/10.1016/j.pepi.2011.03.008>
- Calvo-Rathert, M., Goguitchaichvili, A., & Vegas-Tubía, N. (2009). A paleointensity study on middle Miocene to Pliocene volcanic rocks from south-eastern Spain. *Earth, Planets and Space*, 61(1), 61–69. <https://doi.org/10.1186/BF03352885>
- Camps, P., Henry, B., Prévot, M., & Faynot, L. (2001). Geomagnetic paleosecular variation recorded in Plio-Pleistocene volcanic rocks from Possession Island (Crozet Archipelago, southern Indian Ocean). *Journal of Geophysical Research*, 106(B2), 1961–1971. <https://doi.org/10.1029/2000JB900370>
- Carlut, J., Quidelleur, X., Courtillot, V., & Boudon, G. (2000). Paleomagnetic directions and K/Ar dating of 0 to 1 Ma lava flows from La Guadeloupe Island (French West Indies): Implications for time-averaged field models. *Journal of Geophysical Research*, 105(B1), 835–849. <https://doi.org/10.1029/1999JB900238>

- Ceja, M. R., Goguitchaichvili, A., Calvo-Rathert, M., Morales-Contreras, J., Alva-Valdivia, L., Elguera, J. R., et al. (2006). Paleomagnetism of the Pleistocene Tequila Volcanic Field (Western Mexico). *Earth, Planets and Space*, 58(10), 1349–1358. <https://doi.org/10.1186/BF03352631>
- Chauvin, A., Gillot, P. Y., & Bonhommet, N. (1991). Paleointensity of the Earth's magnetic field recorded by two late Quaternary volcanic sequences at the Island of La Réunion (Indian Ocean). *Journal of Geophysical Research*, 96(B2), 1981–2006. <https://doi.org/10.1029/90JB02223>
- Coe, R. S., Zhao, X., Lyons, J., Pluhar, C., & Mankinen, E. (2000). Revisiting the 1964 collection of Nunivak lava flows. *Eos, Transactions American Geophysical Union*, 81(48). Fall Meeting Suppl., Abstract GP62A-06.
- Conte-Fasano, G., Urrutia-Fucugauchi, J., Goguitchaichvili, A., & Morales-Contreras, J. (2006). Low-latitude paleosecular variation and the time-averaged field during the Late Pliocene and Quaternary-paleomagnetic study of the Michoacan-Guanajuato volcanic field, Central Mexico. *Earth, Planets and Space*, 58(10), 1359–1371. <https://doi.org/10.1186/BF03352632>
- Cromwell, G., Constable, C. G., Staudigel, H., Tauxe, L., & Gans, P. (2013). Revised and updated paleomagnetic results from Costa Rica. *Geochemistry, Geophysics, Geosystems*, 14(9), 3379–3388. <https://doi.org/10.1002/ggge.20199>
- Di Chiara, A., Speranza, F., Porreca, M., Pimentel, A., D'Ajello Caracciolo, F., & Pacheco, J. (2014). Constraining chronology and time-space evolution of Holocene volcanic activity on the Capelo Peninsula (Faial Island, Azores): The paleomagnetic contribution. *Geological Society of America Bulletin*, 126(9–10), 1164–1180. <https://doi.org/10.1130/B30933.1>
- Døssing, A., Muxworthy, A. R., Supakulopas, R., Riisshuus, M. S., & Mac Niocaill, C. (2016). High northern geomagnetic field behavior and new constraints on the Gilsá event: Paleomagnetic and  $^{40}\text{Ar}/^{39}\text{Ar}$  results of ~0.5–3.1 Ma basalts from Jökuldalur, Iceland. *Earth and Planetary Science Letters*, 456, 98–111. <https://doi.org/10.1016/j.epsl.2016.09.022>
- Døssing, A., Riisshuus, M. S., Mac Niocaill, C., Muxworthy, A. R., & MacLennan, J. (2020). Late Miocene to late Pleistocene geomagnetic secular variation at high northern latitudes. *Geophysical Journal International*, 222(1), 86–102. <https://doi.org/10.1093/gji/ggaa148>
- Elmaleh, A., Valet, J. P., Quidelleur, X., Solihin, A., Bouquerel, H., Tesson, T., et al. (2004). Palaeosecular variation in Java and Bawean Islands (Indonesia) during the Brunhes chron. *Geophysical Journal International*, 157(1), 441–454. <https://doi.org/10.1111/j.1365-246X.2004.02197.x>
- Goguitchaichvili, A., Calvo, M., Sologashvili, D., Alva, L., & Urrutia, J. (2000). Palaeomagnetism of Georgian Plio-Quaternary volcanic provinces (Southern Caucasus): A pilot study. *Comptes Rendus de l'Academie des Sciences-Series IIA: Earth and Planetary Science*, 331(11), 683–690. [https://doi.org/10.1016/S1251-8050\(00\)01471-3](https://doi.org/10.1016/S1251-8050(00)01471-3)
- Goguitchaichvili, A., González, J. A., Pluhar, C. J., Alva-Valdivia, L., Rosas Elguera, J., Ruiz-Martínez, V. C., et al. (2011). A comprehensive rock-magnetic, paleomagnetic, paleointensity and geochronology study along the western Trans-Mexican Volcanic Belt: Geodynamic and geomagnetic implications. *Geofísica Internacional*, 50(2), 227–254.
- Goguitchaichvili, A., Petronille, M., Henry, B., Valdivia, L. A., Morales, J., & Urrutia-Fucugauchi, J. (2007). Paleomagnetism of the Eastern Alkaline Province (Mexico): Contribution to the time-averaged field global database and geomagnetic instability time scale. *Earth, Planets and Space*, 59(7), 775–783. <https://doi.org/10.1186/BF03352740>
- Goguitchaichvili, A., Valdivia, L. M. A., Elguera, J. R., Fucugauchi, J. U., Cervantes, M. A., & Morales, J. (2002). Paleosecular variation record of geomagnetic full vector during late Miocene, from the Nayarit area, Mexico. *Physics of the Earth and Planetary Interiors*, 134(1–2), 71–88. [https://doi.org/10.1016/S0031-9201\(02\)00096-1](https://doi.org/10.1016/S0031-9201(02)00096-1)
- Gonzalez, S., Sherwood, G., Böhnell, H., & Schnepf, E. (1997). Palaeosecular variation in Central Mexico over the last 30,000 years: The record from lava flows. *Geophysical Journal International*, 130(1), 201–219. <https://doi.org/10.1111/j.1365-246X.1997.tb00999.x>
- Herrero-Bervera, E., & Valet, J. P. (2002). Paleomagnetic secular variation of the Honolulu Volcanic Series (33–700 ka), O'ahu (Hawaii). *Physics of the Earth and Planetary Interiors*, 133(1–4), 83–97. [https://doi.org/10.1016/S0031-9201\(02\)00092-4](https://doi.org/10.1016/S0031-9201(02)00092-4)
- Herrero-Bervera, E., & Valet, J. P. (2007). Holocene paleosecular variation from dated lava flows on Maui (Hawaii). *Physics of the Earth and Planetary Interiors*, 161(3–4), 267–280. <https://doi.org/10.1016/j.pepi.2007.02.008>
- Johnson, C. L., Wijbrans, J. R., Constable, C. G., Gee, J., Staudigel, H., Tauxe, L., et al. (1998).  $^{40}\text{Ar}/^{39}\text{Ar}$  ages and paleomagnetism of São Miguel lavas, Azores. *Earth and Planetary Science Letters*, 160(3–4), 637–649. [https://doi.org/10.1016/S0012-821X\(98\)00117-4](https://doi.org/10.1016/S0012-821X(98)00117-4)
- Kent, D. V., Wang, H., & Rochette, P. (2010). Equatorial paleosecular variation of the geomagnetic field from 0 to 3 Ma lavas from the Galapagos Islands. *Physics of the Earth and Planetary Interiors*, 183(3–4), 404–412. <https://doi.org/10.1016/j.pepi.2010.08.010>
- Kirschvink, J. L. (1980). The least-squares line and plane and the analysis of palaeomagnetic data. *Geophysical Journal of the Royal Astronomical Society*, 62, 699–718. <https://doi.org/10.1111/j.1365-246X.1980.tb02601.x>
- Kissel, C., Rodriguez-Gonzalez, A., Laj, C., Perez-Torrado, F., Carracedo, J. C., Wandres, C., & Guillou, H. (2015). Paleosecular variation of the earth magnetic field at the Canary Islands over the last 15 ka. *Earth and Planetary Science Letters*, 412, 52–60. <https://doi.org/10.1016/j.epsl.2014.12.031>
- Laj, C., Guillou, H., Szeremeta, N., & Coe, R. (1999). Geomagnetic paleosecular variation at Hawaii around 3 Ma from a sequence of 107 lava flows at Kaena Point (Oahu). *Earth and Planetary Science Letters*, 170(4), 365–376. [https://doi.org/10.1016/S0012-821X\(99\)00119-3](https://doi.org/10.1016/S0012-821X(99)00119-3)
- Laj, C., Rais, A., Surmont, J., Gillot, P. Y., Guillou, H., Kissel, C., & Zanella, E. (1997). Changes of the geomagnetic field vector obtained from lava sequences on the island of Vulcano (Aeolian Islands, Sicily). *Physics of the Earth and Planetary Interiors*, 99(3–4), 161–177. [https://doi.org/10.1016/S0031-9201\(96\)03221-9](https://doi.org/10.1016/S0031-9201(96)03221-9)
- Leonhardt, R., Matzka, J., & Menor, E. A. (2003). Absolute paleointensities and paleodirections of Miocene and Pliocene lavas from Fernando de Noronha, Brazil. *Physics of the Earth and Planetary Interiors*, 139(3–4), 285–303. <https://doi.org/10.1016/j.pepi.2003.09.008>
- Leonhardt, R., & Soffel, H. C. (2006). The growth, collapse and quiescence of Teno volcano, Tenerife: New constraints from paleomagnetic data. *International Journal of Earth Sciences*, 95(6), 1053–1064. <https://doi.org/10.1007/s00531-006-0089-3>
- Lerner, G. A., Cronin, S. J., Turner, G. M., & Rowe, M. C. (2019). Paleomagnetic determination of the age and properties of the 1780–1800 AD dome effusion/collapse episode of Mt. Taranaki, New Zealand. *Bulletin of Volcanology*, 81(3), 15. <https://doi.org/10.1007/s00445-019-1275-z>
- Mahgoub, A. N., Böhnell, H., Siebe, C., Salinas, S., & Guilbaud, M. N. (2017). Paleomagnetically inferred ages of a cluster of Holocene monogenetic eruptions in the Tacámbaro-Puruarán area (Michoacán, México): Implications for volcanic hazards. *Journal of Volcanology and Geothermal Research*, 347, 360–370. <https://doi.org/10.1016/j.jvolgeores.2017.10.004>
- Mahgoub, A. N., Juárez-Arriaga, E., Böhnell, H., Siebe, C., & Pavón-Carrasco, F. J. (2019). Late-Quaternary secular variation data from Mexican volcanoes. *Earth and Planetary Science Letters*, 519, 28–39. <https://doi.org/10.1016/j.epsl.2019.05.001>
- Mahgoub, A. N., Reyes-Guzmán, N., Böhnell, H., Siebe, C., Pereira, G., & Dorison, A. (2018). Paleomagnetic constraints on the ages of the Holocene Malpais de Zacapu lava flow eruptions, Michoacán (México): Implications for archeology and volcanic hazards. *The Holocene*, 28(2), 229–245. <https://doi.org/10.1177/0959683617721323>

- Mejia, V., Barendregt, R. W., & Opdyke, N. D. (2002). Paleosecular variation of Brunhes age lava flows from British Columbia, Canada. *Geochemistry, Geophysics, Geosystems*, 3(12), 1–14. <https://doi.org/10.1029/2002GC000353>
- Mejia, V., Böhnell, H., Opdyke, N. D., Ortega-Rivera, M. A., Lee, J. K. W., & Aranda-Gomez, J. J. (2005). Paleosecular variation and time-averaged field recorded in late Pliocene–Holocene lava flows from Mexico. *Geochemistry, Geophysics, Geosystems*, 6(7). <https://doi.org/10.1029/2004GC000871>
- Mejia, V., Opdyke, N. D., Vilas, J. F., Singer, B. S., & Stoner, J. S. (2004). Plio-Pleistocene time-averaged field in southern Patagonia recorded in lava flows. *Geochemistry, Geophysics, Geosystems*, 5(3). <https://doi.org/10.1029/2003GC000633>
- Michalk, D. M., Böhnell, H. N., Nowaczyk, N. R., Aguirre-Diaz, G. J., López-Martínez, M., Ownby, S., & Negendank, J. F. (2013). Evidence for geomagnetic excursions recorded in Brunhes and Matuyama Chron lavas from the trans-Mexican volcanic belt. *Journal of Geophysical Research*, 118(6), 2648–2669. <https://doi.org/10.1002/jgrb.50214>
- Miki, M., Inokuchi, H., Yamaguchi, S., Matsuda, J. I., Nagao, K., Isezaki, N., & Yaskawa, K. (1998). Geomagnetic paleosecular variation in Easter Island, the southeast Pacific. *Physics of the Earth and Planetary Interiors*, 106(1–2), 93–101. [https://doi.org/10.1016/S0031-9201\(97\)00106-4](https://doi.org/10.1016/S0031-9201(97)00106-4)
- Mitchell, R. J., Jaeger, D. J., Diehl, J. F., & Hammond, P. E. (1989). Palaeomagnetic results from the Indian Heaven volcanic field, south-central Washington. *Geophysical Journal International*, 97(3), 381–390. <https://doi.org/10.1111/j.1365-246X.1989.tb00509.x>
- Monster, M. W., Van Galen, J., Kuiper, K. F., Dekkers, M. J., & De Groot, L. V. (2018). A Late-Quaternary full-vector geomagnetic record from El Golfo section, El Hierro, Canary Islands. *Geophysical Journal International*, 215(3), 1701–1717. <https://doi.org/10.1093/gji/ggy361>
- Oliva-Urcia, B., Gil-Peña, I., Maestro, A., López-Martínez, J., Galindo-Zaldívar, J., Soto, et al. (2016). Paleomagnetism from Deception Island (South Shetlands archipelago, Antarctica), new insights into the interpretation of the volcanic evolution using a geomagnetic model. *International Journal of Earth Sciences*, 105(5), 1353–1370. <https://doi.org/10.1007/s00531-015-1254-3>
- Opdyke, N. D., Kent, D. V., Huang, K., Foster, D. A., & Patel, J. P. (2010). Equatorial paleomagnetic time-averaged field results from 0–5 Ma lavas from Kenya and the latitudinal variation of angular dispersion. *Geochemistry, Geophysics, Geosystems*, 11(5). <https://doi.org/10.1029/2009GC002863>
- Opdyke, N. D., & Musgrave, R. (2004). Paleomagnetic results from the Newer Volcanics of Victoria: Contribution to the Time Averaged Field Initiative. *Geochemistry, Geophysics, Geosystems*, 5(3). <https://doi.org/10.1029/2003GC000632>
- Panaiotu, C. G., Jicha, B. R., Singer, B. S., Tugui, A., Seghedi, I., Panaiotu, A. G., & Necula, C. (2013). <sup>40</sup>Ar/<sup>39</sup>Ar chronology and paleomagnetism of Quaternary basaltic lavas from the Perșani Mountains (East Carpathians). *Physics of the Earth and Planetary Interiors*, 221, 1–14. <https://doi.org/10.1016/j.pepi.2013.06.007>
- Panaiotu, C. G., Visan, M., Tugui, A., Seghedi, I., & Panaiotu, A. G. (2012). Palaeomagnetism of the South Harghita volcanic rocks of the East Carpathians: Implications for tectonic rotations and palaeosecular variation in the past 5 Ma. *Geophysical Journal International*, 189(1), 369–382. <https://doi.org/10.1111/j.1365-246X.2012.05394.x>
- Peña, R. M., Goguitchaichvili, A., Guilbaud, M. N., Martínez, V. C. R., Rathert, M. C., Siebe, C., et al. (2014). Paleomagnetic secular variation study of Ar–Ar dated lavas flows from Tacambaro Area (Central Mexico): Possible evidence of Intra-Jaramillo geomagnetic excursion in volcanic rocks. *Physics of the Earth and Planetary Interiors*, 229, 98–109. <https://doi.org/10.1016/j.pepi.2014.01.005>
- Peña, R. M., Goguitchaichvili, A., Henry, B., Sánchez-Bettucci, L., Morales, J., Reyes, B., et al. (2011). Plio-Pleistocene paleomagnetic record from the Michoacán-Guanajuato monogenetic volcanic field (Western Mexico). *Studia Geophysica et Geodaetica*, 55(2), 311–328. <https://doi.org/10.1007/s11200-011-0017-2>
- Petronille, M., Goguitchaichvili, A., Henry, B., Alva-Valdivia, L. M., Rosas-Elguera, J., Urrutia-Fucugauchi, J., et al. (2005). Paleomagnetism of Ar–Ar dated lava flows from the Ceboruco-San Pedro volcanic field (western Mexico): Evidence for the Matuyama-Brunhes transition precursor and a fully reversed geomagnetic event in the Brunhes chron. *Journal of Geophysical Research*, 110(B8). <https://doi.org/10.1029/2004JB003321>
- Pinton, A., Giordano, G., Speranza, F., & Þórðarson, Þ. (2018). Paleomagnetism of Holocene lava flows from the Reykjanes Peninsula and the Tungnaá lava sequence (Iceland): Implications for flow correlation and ages. *Bulletin of Volcanology*, 80(1), 10. <https://doi.org/10.1007/s00445-017-1187-8>
- Quidelleur, X., Carlut, J., Tchilinguirian, P., Germa, A., & Gillot, P. Y. (2009). Paleomagnetic directions from mid-latitude sites in the southern hemisphere (Argentina): Contribution to time averaged field models. *Physics of the Earth and Planetary Interiors*, 172(3–4), 199–209. <https://doi.org/10.1016/j.pepi.2008.09.012>
- Rais, A., Laj, C., Surmont, J., Gillot, P. Y., & Guillou, H. (1996). Geomagnetic field intensity between 70 000 and 130 000 years BP from a volcanic sequence on La Réunion, Indian Ocean. *Earth and Planetary Science Letters*, 140(1–4), 173–189. [https://doi.org/10.1016/0012-821X\(96\)00024-6](https://doi.org/10.1016/0012-821X(96)00024-6)
- Ricci, J., Carlut, J., & Valet, J. P. (2018). Paleosecular variation recorded by Quaternary lava flows from Guadeloupe Island. *Scientific Reports*, 8(1), 1–14. <https://doi.org/10.1038/s41598-018-28384-z>
- Rodríguez-Trejo, A., Alva-Valdivia, L. M., & Vidal-Solano, J. R. (2019). Paleomagnetism and rock magnetic properties of Late Pleistocene volcanism from El Pinacate Volcanic Field, northwest Mexico. *Journal of South American Earth Sciences*, 96, 102368. <https://doi.org/10.1016/j.jsames.2019.102368>
- Roperch, P., Chauvin, A., Lara, L. E., & Moreno, H. (2015). Secular variation of the Earth's magnetic field and application to paleomagnetic dating of historical lava flows in Chile. *Physics of the Earth and Planetary Interiors*, 242, 65–78. <https://doi.org/10.1016/j.pepi.2015.03.005>
- Ruiz-Martínez, V. C., Urrutia-Fucugauchi, J., & Osete, M. L. (2010). Palaeomagnetism of the Western and Central sectors of the Trans-Mexican volcanic belt—Implications for tectonic rotations and palaeosecular variation in the past 11 Ma. *Geophysical Journal International*, 180(2), 577–595. <https://doi.org/10.1111/j.1365-246X.2009.04447.x>
- Sánchez-Duque, A., Mejia, V., Opdyke, N. D., Huang, K., & Rosales-Rivera, A. (2016). Plio-Pleistocene paleomagnetic secular variation and time-averaged field: Ruiz-Tolima volcanic chain, Colombia. *Geochemistry, Geophysics, Geosystems*, 17(2), 538–549. <https://doi.org/10.1002/2015GC006149>
- Stone, D. B., & Layer, P. W. (2006). Paleosecular variation and GAD studies of 0–2 Ma flow sequences from the Aleutian Islands, Alaska. *Geochemistry, Geophysics, Geosystems*, 7(4). <https://doi.org/10.1029/2005GC001007>
- Tanaka, H., Kamizaki, R., & Yamamoto, Y. (2007). Palaeomagnetism of the Older Ontake Volcano, Japan: Contributions to the palaeosecular variation for 750–400 Ka, the lower half of the Brunhes Chron. *Geophysical Journal International*, 169(1), 81–90. <https://doi.org/10.1111/j.1365-246X.2006.03306.x>
- Tanaka, H., Kawamura, K. I., Nagao, K., & Houghton, B. F. (1997). K–Ar ages and paleosecular variation of direction and intensity from Quaternary lava sequences in the Ruapehu Volcano, New Zealand. *Journal of Geomagnetism and Geoelectricity*, 49(4), 587–599. <https://doi.org/10.5636/jjgg.49.587>

- Tanaka, H., & Kobayashi, T. (2003). Paleomagnetism of the late Quaternary Ontake Volcano, Japan: Directions, intensities, and excursions. *Earth, Planets and Space*, 55(4), 189–202. <https://doi.org/10.1186/BF03351748>
- Tanaka, H., Komuro, N., & Turner, G. M. (2009). Palaeosecular variation for 0.1–21 Ka from the Okataina Volcanic Centre, New Zealand. *Earth, Planets and Space*, 61(1), 213–225. <https://doi.org/10.1186/BF03352901>
- Tanty, C., Carlut, J., Valet, J. P., & Germa, A. (2015). Palaeosecular variation recorded by 9 ka to 2.5-Ma-old lavas from Martinique Island: New evidence for the La Palma aborted reversal ~617 ka ago. *Geophysical Journal International*, 200(2), 917–934. <https://doi.org/10.1093/gji/ggu423>
- Tauxe, L., Constable, C., Johnson, C. L., Koppers, A. A., Miller, W. R., & Staudigel, H. (2003). Paleomagnetism of the southwestern USA recorded by 0–5 Ma igneous rocks. *Geochemistry, Geophysics, Geosystems*, 4(4). <https://doi.org/10.1029/2002GC000343>
- Tauxe, L., Lusk, C., Selkin, P., Gans, P., & Calvert, A. (2004). Paleomagnetic results from the Snake River Plain: Contribution to the time-averaged field global database. *Geochemistry, Geophysics, Geosystems*, 5(8). <https://doi.org/10.1029/2003GC000661>
- Tauxe, L., Staudigel, H., & Wijbrans, J. R. (2000). Paleomagnetism and <sup>40</sup>Ar/<sup>39</sup>Ar ages from La Palma in the Canary Islands. *Geochemistry, Geophysics, Geosystems*, 1(9). <https://doi.org/10.1029/2000GC000063>
- Udagawa, S., Kitagawa, H., Gudmundsson, A., Hiroi, O., Koyaguchi, T., Tanaka, H., et al. (1999). Age and magnetism of lavas in Jökuldalur area, Eastern Iceland: Gilsá event revisited. *Physics of the Earth and Planetary Interiors*, 115(2), 147–171. [https://doi.org/10.1016/S0031-9201\(99\)00073-4](https://doi.org/10.1016/S0031-9201(99)00073-4)
- Yamamoto, Y., Tsunakawa, H., Shaw, J., & Kono, M. (2007). Paleomagnetism of the Datong Monogenetic volcanoes in China: Paleodirection and paleointensity during the middle to early Brunhes Chron. *Earth, Planets and Space*, 59(7), 727–746. <https://doi.org/10.1186/BF03352736>
- Zijderveld, J. D. A. (1967). AC demagnetization of rocks: Analysis of results. In D. W. Collinson, K. M. Creer, & S. K. Runcorn (Eds.), *Methods in palaeomagnetism*. Elsevier.